Engineering Structures 353 (2026) 122203

Contents lists available at ScienceDirect

Engineering Structures

journal homepage: www.elsevier.com/locate/engstruct

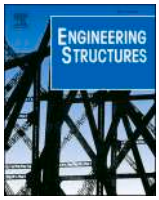

Crowdsensing-based automated operational modal analysis for indirect bridge structural health monitoring

Eleonora Massarelli [a], Marco Civera [a,*], Samuele Mara [b], Marco Raimondi [c], Pier Francesco Giordano [d], Said Quqa [e], Mauro Aimar [a], Maria Pina Limongelli [d], Bernardino Chiaia [a]

[a] Department of Structural, Building and Geotechnical Engineering, Politecnico di Torino, Corso Duca degli Abruzzi 24, Torino 10129, Italy
[b] Istituto Dalle Molle di Studi sull'intelligenza Artificiale, USI-SUPSI, Via la Santa 1, CH-6962 Lugano-Viganello, Switzerland
[c] Department of Electronics, Information and Bioengineering, Politecnico di Milano, Piazza Leonardo da Vinci 32, 20133 Milan, Italy
[d] Department of Architecture, Built Environment and Construction Engineering, Politecnico di Milano, Piazza Leonardo da Vinci 32, Milan 20133, Italy
[e] Department of Civil, Chemical, Environmental, and Materials Engineering, University of Bologna, Viale del Risorgimento 2, Bologna 40136, Italy

ARTICLE INFO

Keywords:
Indirect structural health monitoring
Drive-by bridge monitoring
Automated operational modal analysis
Mobile crowdsensing
Machine learning
Data fusion
Footbridge

ABSTRACT

In this study, an automated identification procedure for crowdsensing-based indirect Bridge Structural Health Monitoring (iBSHM) is presented. The scope is to estimate the modal parameters of a cycle-pedestrian bridge using only acceleration data collected by smartphones installed on board. The proposed method introduces several innovations. First, natural frequencies are identified using the Stochastic Subspace Identification (SSI) algorithm. Second, the method enables the estimation of damping ratios, which are typically neglected in existing crowdsensing applications. Third, it uses the Singular Value Decomposition (SVD) step within the SSI framework to extract singular vectors corresponding to dominant frequencies, thereby isolating the modal components of the signal and enabling the estimation of mode shapes. The proposed identification procedure is experimentally tested and validated with data from a real footbridge in Bologna (Italy). The field test was carried out with multiple passages of a commercial bicycle, using a single smartphone installed on board. The obtained results are compared with those from a previous test conducted with the same experimental setup and case study, but using a different analysis methodology. Satisfactory comparability and repeatability of the results were achieved.

1. Introduction

The ageing of both long- and short-span bridges in Italy, combined with increasing loading demands, has heightened significant concerns over potential serviceability losses and structural failures. This situation highlights the urgent need for effective bridge Structural Health Monitoring (SHM) systems, which are essential for detecting early-stage damage and addressing these newly arising challenges. In this regard, monitoring changes in modal parameters over time serves as a valuable indicator of potential structural deterioration [1], enabling predictions of a bridge's remaining service life and improving infrastructure management efficiency. However, traditional vibration-based SHM depends on networks of fixed sensors installed on the structure to collect vibration data under operating conditions. While this approach is well established and proven, the high costs of installing and maintaining permanent systems limit their deployment to a select number of strategic or high-risk structures.

Drive-by SHM, also known as indirect Bridge Structural Health Monitoring (iBSHM), offers an interesting alternative to direct SHM. In this framework, data are collected by sensors mounted on a moving vehicle; since one instrumented vehicle can collect data from multiple bridges, this approach offers a more cost-effective paradigm for bridge monitoring. This technique relies on the principle that the instrumented vehicle and the bridge form a coupled dynamic system, in which data collected on the vehicle inherently contain information about the bridge's properties. The concept of iBSHM is rapidly rising, as it has been finally enabled by recent progress in signal processing and pattern recognition algorithms [2], especially in the field of crowdsensing, where changes in modal parameters are investigated with multiple acquisition runs on the bridge. Besides, because the sensing vehicle

* Corresponding author.
E-mail address: marco.civera@polito.it (M. Civera).

https://doi.org/10.1016/j.engstruct.2026.122203
Received 3 August 2025; Received in revised form 7 January 2026; Accepted 18 January 2026
Available online 27 January 2026

moves longitudinally across the entire deck, iBSHM can provide more spatially detailed and comprehensive information. Importantly, iBSHM should not be viewed as a complete replacement for direct SHM methods, but rather as a complementary tool to enhance early damage detection and reduce monitoring costs. Its rapid deployment and flexible application make it especially suitable for large-scale preliminary screening, enabling the prioritisation of bridges that require further investigation using conventional direct SHM techniques.

1.1. State of the Art in Indirect Bridge Structural Health Monitoring

In this context, in 2004, Yang et al. [3] introduced the idea of extracting the bridge's modal properties from a passing vehicle. They used a simplified vehicle-bridge interaction (VBI) model to validate the concept theoretically, then verified it through a first field experiment using a tailored prototype [4].

However, using a moving instrumented vehicle for bridge SHM presents some inherent challenges, e.g., the noise related to different sources such as the engine, the suspension, and the shock absorbers [5], as well as the road pavement roughness and damage-unrelated confounding influences (e.g., temperature fluctuations [6]). Several authors have addressed these limitations in the literature, each one suggesting different ways to mitigate them. For instance, noise due to the road pavement roughness can be reduced through the simultaneous use of multiple testing vehicles to compensate for the detrimental effects [7]. Some authors [8-10] developed methods to limit the effects of pitch and roll motions in the vehicle, which could hide the bridge response collected on the vehicle itself. Appropriate sensor placement appears to be an optimal solution to compensate for such undesirable effects. On the other hand, engine noise can be mitigated by using a hybrid or electric vehicle [11]. The feasibility of iBSHM has been tested on different bridge structural schemes and by using a wide range of test vehicles, such as instrumented commercial cars with a traditional internal combustion engine [8,9,12,13,14], hybrid [15], and electric ones [11], vans [16], city buses [17,18], trucks [19], bicycles [20], tractor-trailer solutions [4,21,22], trains [23], a prototype of an electric quad [24] and one hand-drawn cart [25]. Of course, as will be shown and discussed here in this work, human-propelled vehicles (HPVs), also known as light vehicles (LVs), are not hampered by engine noise. These vehicles have seen a rapid increase in use, especially in urban areas, meeting the need for agile and low-cost transportation systems that are simultaneously sustainable from an environmental and logistical point of view, having been proven to reduce car use, consequently reducing traffic in city centres [26].

Related to other aspects, a significant number of studies focused on defining the optimal conditions to extract the bridge modal parameters [14,27]. Cerda et al. [28] conducted laboratory tests with varying speed and damage levels, comparing direct and indirect SHM; the results highlighted that the outcome improved linearly with the number of repeated measurements. Additional studies have been conducted, such as parametric studies [29] reconstructing surface roughness and varying vehicle and bridge configurations. Nevertheless, despite the growing amount of dedicated research works, many of these challenges remain unsolved as of this date.

1.2. Drive-by monitoring of footbridges with instrumented HPVs

A first open issue concerns cycle-pedestrian bridges. On these infrastructures, of course, engine vehicles are not allowed. Thus, instrumented LVs are required. These have been much more rarely investigated. A second point regards the cost-effectiveness of the instrumented drive-by SHM solutions. In recent years, researchers have suggested exploiting the increasing performance of modern smartphones for SHM. These studies considered both single-sensor solutions and crowdsensing-based ones. The latter group refers to algorithms that collect large amounts of data from all vehicles passing over the infrastructure. This approach has already been proven efficient in increasing road safety and traffic monitoring [30]. In fact, smartphones, envisioned as wireless sensors, can be employed as low-cost and reliable sensors to assess bridges' health conditions.

Regarding the use of crowdsourced data in drive-by bridge monitoring, Matarazzo et al. [31] collected data on two bridges, the Golden Gate Bridge in California and a medium-span RC bridge in Ciampino, Italy, exploiting a fleet of vehicles that allowed the identification of the modal frequencies and the instantaneous amplitudes. Cronin et al. [32] extended the same method to two other steel bridges with medium-long spans. Quqa et al. [20] proposed an iBSHM solution based on data collected from smartphones temporarily installed on shared micro-mobility vehicles, extending for the first time such methodology to infrastructures not accessible by cars, such as footbridges. More recently, Li et al. [26] proposed a mobile crowdsensing approach employing electric scooters to train convolutional neural networks for damage detection on a footbridge. Feng et al. [33] conducted experimental modal identification of a pedestrian bridge leveraging existing micro-mobility systems. Other authors (e.g., [34-36]) extended these studies by analysing the dynamic characteristics of different vehicles, including buses, cars, and e-scooters, and conducted numerical simulations to assess their impact on bridge modal identification using crowdsourced mobile sensing data. Potentiality for drive-by damage detection was investigated by the "fleet SHM" concept [37,38].

1.3. An automated proposal for iBSHM

To the Authors' current knowledge, most full-scale tests focus on the extraction of natural frequencies, while damping ratios are often entirely dismissed [39]. Regarding mode shapes, these are usually estimated by bandpass filtering the acquired signals in a narrow frequency band centred on the identified natural frequency of interest. As for the extraction of the natural frequencies, the majority of the current studies employ classical (non-automated) operational modal analysis (OMA) algorithms, or simpler solutions, such as Peak Picking (PP) from the Power Spectral Density (PSD) [11,15,20] or the Fourier Transform [16,40] of the vertical acceleration signals in different operating conditions. This research work proposes a method to extract the complete set of modal parameters (natural frequencies, damping ratios, and mode shapes) of lightweight bridges using data collected by smartphones mounted on HPVs. Given the current lack of Automated Operational Modal Analysis (AOMA) in the context of iBSHM, the proposed method introduces an automated approach that implements stochastic dynamics and clustering techniques within a workflow suitable for crowdsensing-based drive-by bridge SHM. The proposal was successfully tested on a real steel-made lightweight bridge in Bologna (Italy) and carried out using a commercial city bicycle instrumented with a smartphone. The work by Quqa et al. [20] will serve as the benchmark for the methodology proposed here, which has been validated in the same case study and aims to incrementally extend the previous work of some of the authors to broaden its scope of application, as discussed in more detail in the following parts of this paper.

The remainder of the paper is organised as follows. In Section 2, the methodology for crowdsensing-based iBSHM modal identification is discussed. The proposed algorithm is detailed, and its relevant theoretical background is presented. Section 3 describes the case study, together with the experimental campaign setup and methods. Section 4 reports the results obtained and compares them to those of the previous field test. Finally, Section 5 concludes this article with the key findings and final considerations.

2. System identification procedure

This study builds on the workflow presented in Quqa et al. [20] by using Automated OMA algorithms in place of peak picking from the PSD of the vertical accelerations. As in that work, acceleration recordings

from commercial smartphones collected during multiple passages over a cycle-pedestrian bridge are used to identify the structure's modal parameters. In addition to natural frequencies and mode shapes identified in [20], this study introduces several innovations, including the estimation of damping ratios. To this aim, an approach based on Stochastic Subspace Identification (SSI) [41] has been applied to identify the first natural frequency and damping ratio of the bridge and retrieve the corresponding mode shape. This procedure, detailed in Fig. 1, consists of the following steps:

(1) Identification of the natural frequencies and damping ratios through SSI.
(2) Extracting the modal components associated with the identified natural frequencies.
(3) Estimating the vehicle trajectory by fusing GPS and Inertial Measurement Unit (IMU) data collected during each vehicle trip.
(4) Identifying the absolute modal amplitude along the vehicle trajectory.
(5) Realigning it with the vehicle position and projecting it on the bridge axis.
(6) Estimating the average mode shapes, natural frequencies, and damping ratios from all runs.

While in Quqa et al. [20] the modal components of interest were isolated using a bandpass filter based on prior knowledge of the structural dynamics, this study proposes an alternative approach that extracts the modal components directly from the results of the SSI algorithm, without the need for any a priori assumptions. The procedure is detailed in Section 2.1.

2.1. Estimating natural frequencies and damping ratios

While SSI algorithms have not yet been applied to micromobility-based iBSHM, they have been explored in drive-by monitoring scenarios involving engine-propelled vehicles. In such contexts, the time-varying nature of the system, caused by the movement of the vehicle and onboard sensors, requires specific adaptations. Yang et al. [43] modified the VBI equations in the state space to adapt the SSI algorithm for extracting the first natural frequencies of the bridge, removing the influence of vehicle dynamics. Exploiting SSI, Li et al. [44] proved through simulations and a laboratory experiment the possibility of using one moving sensor and a fixed one to extract natural frequencies and mode shapes. Other authors proposed a Short-Time SSI algorithm to estimate bridge frequencies, theoretically allowing for time-varying system matrices [45], and a damage detection method exploiting subspace projection of acceleration data from moving vehicles [46].

The underlying idea is the assumption that SSI may apply to time-varying systems, provided that the measured signal remains statistically stationary over the acquisition interval [43], [44]. However, this condition is valid only when the temporal variations of the VBI system are negligible compared to the bridge's structural dynamics. This limitation could become critical for short-span bridges or at high speeds of

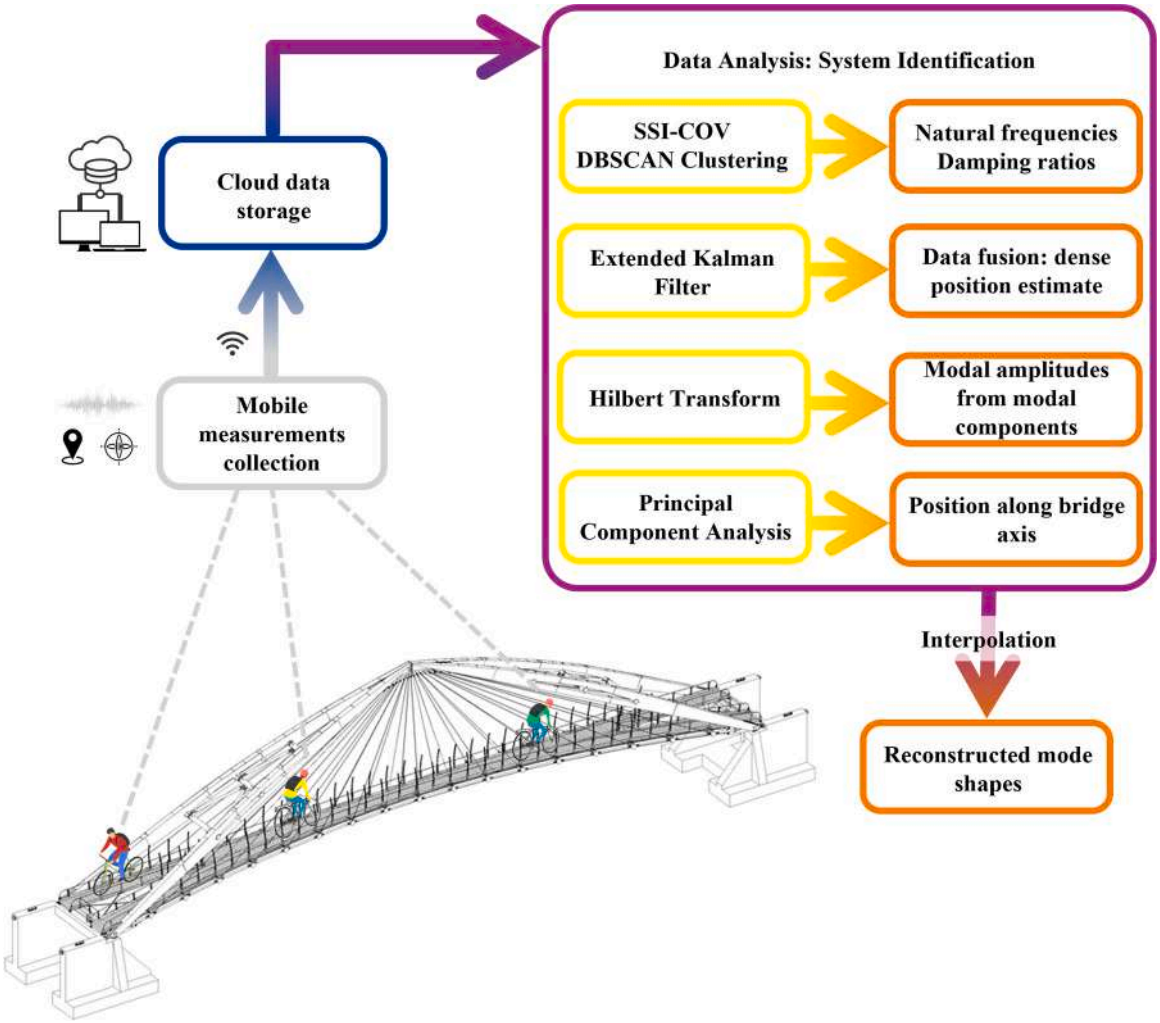

Fig. 1. Workflow of the proposed identification procedure. (3D sketch of the bridge adapted from [42]).

the test vehicle [45], when a shorter signal duration T will reduce the frequency resolution $\Delta f = \frac{1}{T}$. Indeed, past studies indicate that successful frequency identification is achievable when the test vehicle travels at a slow speed, to minimise the time-varying effects of the VBI system [44]. Therefore, if the variation in the VBI dynamics during acquisitions across the bridge is much slower than the dynamics of the structural system, the signal can be assumed stationary in the frequency domain, and the applicability of SSI holds. As it will be proved in the field test results reported here, this was found to be the case for a commercial bicycle running over a mid-sized footbridge.

More specifically, the data-driven version of the algorithm (SSI-DATA) was applied in the present research [47]. Working directly with raw output data, SSI-DATA enables more effective management of noisy data, leading to reliable identifications even with short signals. The discrete-time state space representation of the structural model can be expressed as follows:

$$\mathbf{x_{k+1}} = \mathbf{A}\cdot\mathbf{x_k} + \mathbf{w_k} \tag{1}$$

$$\mathbf{y_k} = \mathbf{C}\cdot\mathbf{x_k} + \mathbf{v_k} \tag{2}$$

where $\mathbf{x_k}$, of dimension $n \times 1$, is the state vector measured at the generic time instant t_k, and $\mathbf{A}$, of dimension $n \times n$, is the state transition matrix. The vector $\mathbf{y_k}$, of dimension $p \times 1$, contains the observed (i.e., measured) quantities at p observation points. The state vector is linked to $\mathbf{y_k}$ via the observation matrix $\mathbf{C}$, of dimension $n \times p$. The two vectors $\mathbf{w_k}$ and $\mathbf{v_k}$ are stochastic processes which model the system and the measurement noise, respectively. Eigenvalues of $\mathbf{A}$, which are related to the poles of the system, depend on the model order n chosen to model the system.

Assuming that the time variations of the VBI system are negligible compared to the bridge dynamics, all matrices and vectors are treated as approximately linear time-invariant. This assumption enables the direct application of standard SSI algorithms to moving sensor data while maintaining their theoretical validity. The p output measurements are gathered into the block Hankel matrix $\mathbf{H}$, which has (as conventional) $2i$ block rows and j columns. This matrix can be divided into two sub-matrices, which represent the 'past' and 'future' input data, respectively $\mathbf{Y_{hp}}$ and $\mathbf{Y_{hf}}$. In this framework, a fundamental step involves working with the projection matrix $\mathbf{O_i}$, which is obtained by projection of the future part of the Hankel matrix into its past part [41] as:

$$\mathbf{O_i} = \mathrm{E}(\mathbf{Y_{hf}}|\mathbf{Y_{hp}}) \tag{3}$$

The matrix $\mathbf{O_i}$ is correlated to the observability matrix $\mathbf{\Gamma_{si}}$ (with n columns) and the initial Kalman state space sequences, collected into the $\widehat{\boldsymbol{X}}_i$ matrix, since the projection matrix can be factorised as the product of such matrices [47] as:

$$\mathbf{O_i} = \mathbf{\Gamma_{si}}\widehat{\mathbf{X}}_\mathbf{i} \tag{4}$$

The Singular Value Decomposition (SVD) is then applied to the projection matrix, obtaining

$$\mathbf{O_i} = \mathbf{USV^T} \tag{5}$$

where $\mathbf{U}$, of dimension $2ip \times n$, and $\mathbf{V}$, of dimension $j \times n$, are the orthogonal matrices corresponding to the left and right singular vectors, and $\mathbf{S}$, of dimension $n \times n$, is the diagonal matrix of singular values, where n represents also the number of non-zero singular values, thus the decoupled components identified through SVD. From that, the observability and Kalman state matrices $\mathbf{\Gamma_{si}}$, $\widehat{\mathbf{X}}_\mathbf{i}$ are computed by inverting Eq. 4:

$$\mathbf{\Gamma_{si}} = \mathbf{US^{1/2}} \quad ; \quad \widehat{\mathbf{X}}_\mathbf{i} = \mathbf{S^{1/2}V^T} \tag{6}$$

In turn, $\mathbf{\Gamma_{si}}$ serves to estimate the system matrices $\mathbf{A}$ and $\mathbf{C}$, from which the modal parameters of the system are then extracted, starting from eigenvalue decomposition of $\mathbf{A}$:

$$\mathbf{A} = \mathbf{\Psi\Lambda_d\Psi^{-1}} \tag{7}$$

The eigenfrequencies ω_i and damping ratios ξ_i are computed from the discrete time eigenvalues μ_i contained in the eigenvector matrix $\mathbf{\Lambda_d}$ as:

$$\omega_i = |\lambda_i| = \left|\frac{\ln(\mu_i)}{\Delta t}\right|; \quad \xi_i = \frac{\mathrm{Re}(\lambda_i)}{|\lambda_i|} \tag{8}$$

It is noteworthy to point out that, when applying SSI to iBSHM problems, only one acquisition position (i.e., the vehicle) is available; if considering only the vertical direction, that means just one channel and one output-only time series ($p = 1$), which is moving in space over time along a defined trajectory. This configuration does not affect the estimation of the natural frequencies and damping ratios, as they do not depend on the sensor locations. However, the modal matrix $\mathbf{\Phi} = [\boldsymbol{\phi}_1; \ldots; \boldsymbol{\phi}_n]$ (i.e., the matrix containing the estimated modal shapes, represented by the vectors $\boldsymbol{\phi}_i$) will collapse into a $1 \times n$ vector. This impairs the direct extraction of mode shapes, since the sole modal coordinate is inherently of unit value. For this reason, the steps outlined in the following paragraphs are implemented to estimate approximate mode shapes from a moving sensor.

At the end of the System Identification procedure described above, SSI returns all the identified poles. Since the number of relevant degrees of freedom is not known a priori, this process is generally repeated for a range of increasing model orders; then, all the results are usually represented in a stabilisation diagram, i.e., a plot of the natural frequencies and damping ratios relative to the model orders. These comprehend the physical modes as well as the spurious and mathematical ones. Several methods to automate the physical modal parameter identification have been proposed. In this study, the AOMA procedure introduced by Reynders et al. [48] and refined in successive works by other authors [49,50] was adopted. First, single-mode validation criteria are implemented in two consecutive steps:

- Hard validation criteria, which consist of setting boundary values to ensure that identified poles have physical meaning. In the case of structures, poles with negative or unrealistically high damping ratios (i.e., greater than 20 %) can be labelled as mathematical poles.
- Soft validation criteria, which return the poles labelled as stable or unstable based on different comparison parameters, defined as in [50,51]. These are dimensionless distances measured between the generic j-th pole belonging to the model order n and the generic k-th pole belonging to the next model order $n+2$ (please note that, in the convention used here, the model order equals the number of poles; thus, being the poles complex conjugates, n increases in steps of 2). The distances are evaluated based on the absolute differences between the estimated eigenvalues $d\lambda$, natural frequencies df, and damping ratios $d\xi$.

The successive step concerns classifying the remaining poles as possibly physical or mathematical (i.e., spurious) using a clustering algorithm to group poles characterised by similar modal features. In this work, a density-based clustering approach—Density-Based Spatial Clustering of Applications with Noise (DBSCAN)—is adopted. The detailed implementation steps of DBSCAN are provided in the original study by Ester et al. [52]. This procedure can be automated, as explained in [51]. Given the crowdsensing nature of this methodology, the mean natural frequency and damping ratio are computed for each cluster and for each signal to obtain a set of cluster-representative modal parameters. These mean values are then used in statistical analyses to derive the structure's significant modal parameters through averaging.

2.2. Estimating mode shapes

Regarding the mode shapes, this study investigates the feasibility of leveraging the SVD step in Eq. 5 to separate the signal's dominant

dynamic components. In particular, in the case of $p = 1$ corresponding to a single moving sensor, the observability matrix loses its direct connection to the spatial information and collapses into a vector of dimension $2i \times 1$ for each mode, since $\mathbf{U}$ becomes $2i \times n$. Matrix $\widehat{\mathbf{X}}_\mathbf{i}$ $(n \times j)$, instead, maintains the temporal evolution of each decoupled mode. Because the acquisition channel is moving, the spatial position $y(t)$ associated with each time step t is known, therefore, $\widehat{\mathbf{X}}_\mathbf{i}$ implicitly contains the spatial information. Thus, from Eq. (6), the rows of $\mathbf{V}^\mathbf{T}$ (or equivalently the columns of $\mathbf{V}$) contain the time histories of the single modal coordinate. This enables the direct use of decoupled signal components corresponding to the single mode of interest. That is to say, the matrix of the right singular vectors, $\mathbf{V}$, contains the contributions of each mode to the system's overall response, enabling the extraction of acceleration signal components associated with specific modes and natural frequencies. By isolating the j-th column of $\mathbf{V}$, denoted as $\mathbf{v_j}$, which corresponds to the singular value linked to the natural frequency $f_{n,j}$ previously identified through the AOMA algorithm, it becomes possible to retrieve the signal component associated with that specific mode.

Since these target frequencies are selected based on the most frequently identified natural frequencies, the process of isolating relevant modal components is automated. This eliminates the need for prior knowledge of the structure's dynamic properties and the manual tuning of bandpass filters. As a result, the proposed AOMA-based method supports an automated, two-step approach to modal identification, where the first step is the procedure described in Section 2.1 (to retrieve f_n and ξ_n) and the second step is the one described here to obtain $\boldsymbol{\phi_n}$.

The procedure is detailed as follows. Data fusion between heterogeneous sensors, i.e., the smartphone's accelerometer (IMU) and GPS, is first required to determine the vehicle's trajectory and instantaneous position along the bridge axis. In this work, sensor data fusion is performed using the Continuous-Discrete Extended Kalman Filter (CD-EKF). In this regard, the system state is modelled as continuous, but the observations are acquired at discrete times. This is necessary since the measurements for the correction phase of the filter come from sensors with different and asynchronous sampling rates at discrete times (see [53] for algorithm details). This step of the procedure is defined and implemented as described in [20]. Fig. 2 shows the smartphone sensors and the measurements used in this context.

The concept follows the one presented by Yang et al. [22], who

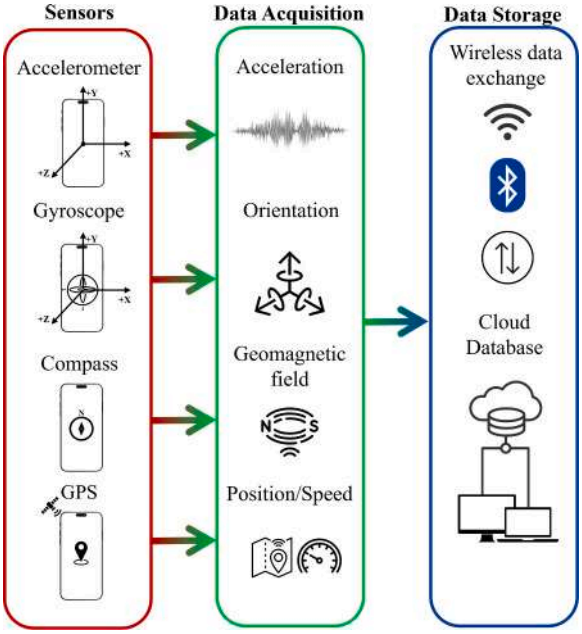

Fig. 2. Smartphone sensors, functionalities, and data storage.

extracted bridge mode shapes from the vertical acceleration response of a scanning vehicle by using the Hilbert Transform (HT) [54], which returns the signal's instantaneous amplitude. The core idea is simple: knowing the vehicle's instantaneous velocity along a known trajectory, it is possible to pinpoint each timestep to a unique location. Then, the instantaneous amplitude of the signal component related to a specific vibration mode will be related to that mode shape's amplitude at the corresponding spatial coordinate. This method has been proven efficient in approximating mode shapes with high spatial resolution, especially in the case of lower speeds of the test vehicle [55], and for structures with well-separated modes. The HT, however, has two main limitations. The first is that the instantaneous amplitude, computed as the modulus (envelope) of the HT's analytical signal, is reported in absolute value. Therefore, it cannot represent negative results, which are mirrored in their positive counterparts. Consequently, the sign information is not encoded in the amplitude; hence, in general, the extracted modal shapes must be interpreted accordingly. The second main difficulty arises from isolating and decoupling the relevant signal component from the recorded time history, since this latter one is a linear combination of multiple modes. In fact, in the context of iBSHM, the signal comes from the vertical acceleration response $\ddot{u}(y,t)$ of the moving test vehicle during its passage over the bridge [56], with y being the longitudinal direction. Using the modal superposition method, it can be expressed in terms of mode shapes $\boldsymbol{\phi_j}(y_k)$, and modal coordinates $q_j(t)$ as follows:

$$\ddot{u}(y,t) = \sum_{j=1}^{\infty} \boldsymbol{\phi_j}(y)\ddot{q}_j(t) \tag{9}$$

Thus, for a given i-th mode, the aim is to retrieve $\boldsymbol{\phi}_{j=i}(y)\ddot{q}_{j=i}(t)$ from $\ddot{u}(y,t)$, discarding all other signal components $(j \neq i)$. What is observed here is that $\mathbf{v_{j=i}} \cong \boldsymbol{\phi}_{j=i}(y)\ddot{q}_{j=i}(t)$ thanks to the properties of SVD previously explained.

Importantly, it is more correct to refer to what is extracted here as operating deflection shapes (ODSs) rather than proper mode shapes. In fact, mode shapes $\boldsymbol{\phi_n}$ are intended as the relative amplitudes of the different modal coordinates, defined up to a constant value and thus not in absolute terms. Conversely, $\mathbf{v_j} \cong \boldsymbol{\phi_j}(y)\ddot{q}_j(t)$ are defined in absolute terms. Hence, the mode shapes $\boldsymbol{\phi_j}(y)$, which are spatial-dependent but time-independent, are only a component in the ODSs $\boldsymbol{\phi_j}(y)\ddot{q}_j(t)$, which are technically time- and space-dependent. However, as said, due to the moving sensor, each instant t can be mapped to a unique position $y(t)$. Furthermore, two considerations can be made. The first regards the single run. It is assumed here that the bridge is naturally excited by random vibrations of equal intensity at the same time and at any point. This is the same assumption at the basis of Ambient Vibration Tests (AVTs), which are the standard for output-only OMA. Thus, under this assumption, the time-dependent terms in the ODSs should be (almost) identical everywhere and always; and therefore, each j-th ODS is approximately equal to an unscaled $\boldsymbol{\phi_j}$. That makes them qualitatively similar, up to an unknown constant, and thus valid for the intended use of this System Identification procedure. The second consideration regards the average of multiple runs. When several HPVs are crossing the same bridge with different speeds and paths, the term $\boldsymbol{\phi_j}(y_k)$ at a generic location y_k remains constant in all acquisitions, while the term $\ddot{q}(t_k)$ varies for each vehicle trip. By exploiting the crowdsensing concept, the proposed procedure is applied for each single run over the bridge; the results obtained from multiple crossings are then averaged, removing the time-dependent components and leaving only the modal instantaneous amplitude $\overline{\boldsymbol{\phi_j}}(y_k)$ for the j-th mode, again defined up to an unknown constant scaling factor. For all these reasons, once the natural frequencies are identified using the SSI method, the corresponding modal amplitudes for each mode can be extracted from the associated singular vectors (see Eq. 5).

At this point, the HT is computed not on the narrowband filtered signal, as done in [20], but directly on the target decoupled acceleration signals v_j from matrix $\mathbf{V}$. The estimated absolute amplitudes are then

converted from time to spatial domain along the bridge axis to be realigned with the actual vehicle positions for each dataset; then, the amplitudes are interpolated with the principal components of the previously estimated trajectory using a user-defined spatial grid along the bridge axis, as reported in detail in [20].

3. Case study: The Bologna A13 footbridge

The field study was selected to examine the feasibility of acquiring crowdsensed data from iBSHM, aiming to perform modal identification of a real lightweight cycle-pedestrian bridge. A typical city bicycle was used as the instrumented HPV to cross the entire footbridge. The data were acquired using a smartphone mounted on the bicycle, serving as the moving sensor. To simulate crowdsourcing, the analysis was repeated by crossing the footbridge several times in both directions, yielding a dataset of 30 runs.

3.1. Footbridge description

The tested structure is a cycle-pedestrian bridge which passes over the A13 Bologna-Padova motorway near the Bologna ring road entrance. Its coordinates are Latitude = 44° 31′ 43.77″ N, Longitude = 11° 21′ 33.08″ E (DMS Format). The solution chosen by the designer is a steel-tied arch structural support system and internal cable staying, covering the entire highway width with a span of more than 90 m. The original plan and lateral views of the project are shown in Fig. 3. As reported in detail in [42,57] the structural system mainly consists of:

- A three-hinged arch main support structural system with a counter-stressed tie mechanism.
- An internal fan-shaped cable stay system supporting the deck structure (Fig. 4 (a)).
- A pre-stressed transversal stabilising system through cables with opposing curvature.
- A foundation system made of reinforced concrete abutments on filled embankments and piles.

Moreover, the deck is characterised by an hourglass shape and presents a slight inclination (Fig. 3). Regarding the road surface, the pavement is made of a plastic material, typical for footbridges, as shown in Fig. 4 (c). This kind of pavement, despite some surface deterioration, still appears smooth and, very importantly, it does not negatively affect the recorded data by causing additional noise. This allowed, as in previous works [20], to avoid considering the effect of the pavement roughness.

Fig. 5 shows the results of traditional tests, aimed at the dynamic characterisation of the structure, as reported in [49]. It can be noticed how, according to this source, the first flexural modes reported are very close in frequency, with only $\Delta f \cong 0.04$ Hz. These two mode shapes clearly represent the first and second vertical bending modes, in this

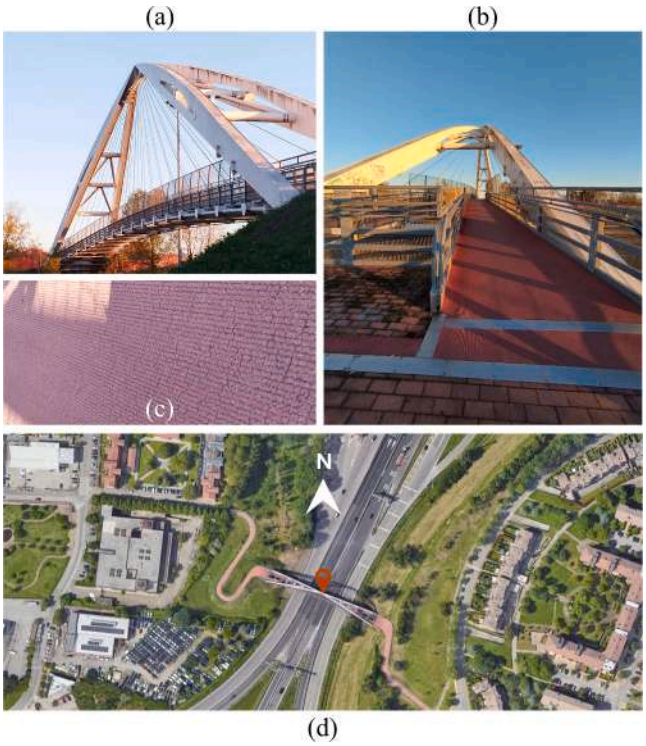

Fig. 4. Footbridge details. Side view (a), front view (b), pavement detail (c), and satellite image with its surroundings (d).

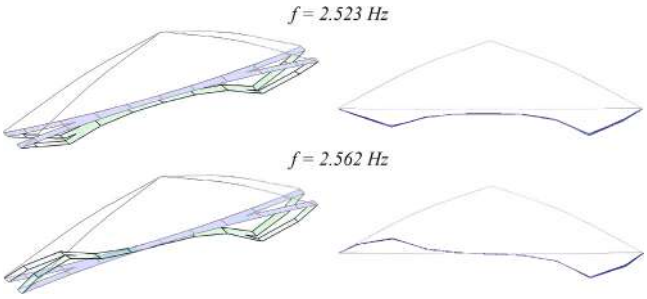

Fig. 5. Modal identification results from previous experimental tests on the selected case study, with 3D view (left) and lateral view (right). Image retrieved from [42].

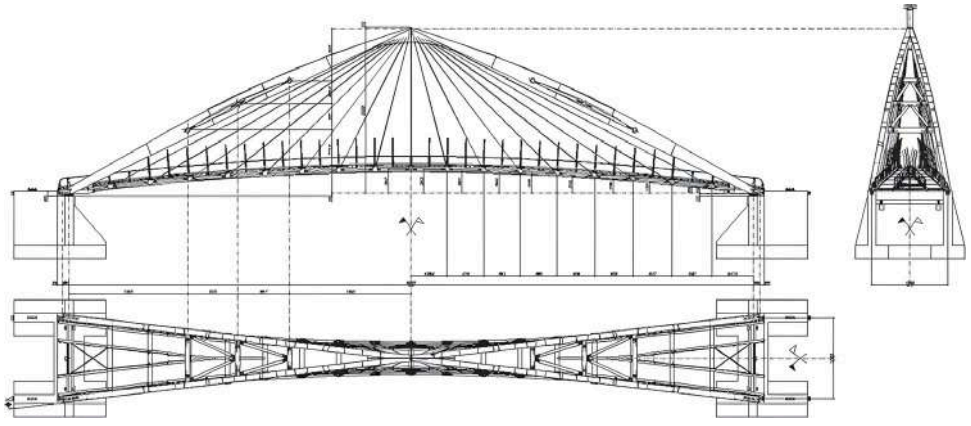

Fig. 3. Plan, lateral, and front views of the footbridge. Technical drawings retrieved from [42].

order. It is noteworthy that only the first two natural frequencies are available to the Authors, while the reference mode shapes could not be retrieved – indeed, Fig. 5 only reports a qualitative sketch of these mode shapes.

3.2. Experimental setup

The experimental campaign on the described cycle-pedestrian bridge was conducted in December 2023. To obtain results directly comparable with the ones previously presented in [20], the experimental setup was recreated as closely as possible. Importantly, this configuration enables crowdsensing-based infrastructure monitoring for shared micromobility vehicles, such as bicycles and scooters. In particular, the same bicycle used in [20] was used for the tests on the footbridge (Fig. 6). Measurements were collected using a commercial smartphone (Xiaomi Redmi Note 11 Pro) mounted on the bicycle frame (Fig. 6 (b)). The sensor configuration was designed to simulate the use of bicycle-sharing vehicles, where a smartphone is required to access the service and can be placed on a support. In this case, the smartphone was mounted to the front tube via a metal support, ensuring a rigid connection to the bicycle's frame. An additional smartphone (iPhone XS) was placed directly on the bridge midspan to act as a conventional (i.e., physically attached) reference sensor.

Regarding the testing conditions, the bicycle tyres were inflated to an internal pressure of about 3 atm. For each run (i.e., one-directional bicycle trip), the sensors were triggered manually. The measurements were acquired using the MATLAB Mobile app. This allows recording, sending, and saving data to the MathWorks Cloud, where the data can be stored and later analysed. Several measurements are needed to implement the presented algorithm, including triaxial acceleration (m/s^2), triaxial angular velocity (rad/s), orientation (azimuth, pitch, and roll) (degrees), and position (latitude, longitude, altitude, and speed). Furthermore, for all these measurements, their horizontal accuracy was measured and stored. All these sensed properties are acquired in accordance with the smartphone's internal reference axes convention (Fig. 6 (c)). The triaxial geomagnetic field, in μT, was similarly recorded, although it proved not useful for this study. Regarding the hardware specifics, the IMU sensors were set to collect data at a sampling rate of 100 Hz, while the GPS was limited to 1 Hz.

For the implementation of the CD-EKF, the measurement noise and process noise variances are required. These values are reported in Table 1. The initial state covariance matrix was assumed to be a diagonal matrix, with elements along the diagonal equal to 10^{-3}. The reference bridge direction (ground truth) and the EKF parameters have been set as in the reference research [20]. Accordingly, lower weights were assigned to the GPS measurements, to account for their lower accuracy and sampling rate, although maintaining their fundamental contribution to trajectory estimation.

A total of 30 runs were performed by making trips back and forth over the footbridge, maintaining the same configuration shown in Fig. 6, to simulate a crowdsensing scenario in which repeated runs represent different users. Since the bicycle was manually driven, the speed suffered from slight changes, ranging from 0.7 to 4.7 m/s, where the extreme values are encountered when entering and exiting the bridge, respectively, as visible in Fig. 7 for the runs in West-East (a) and East-West (b) direction. However, the speed was successfully kept low and reasonably constant for the actual bridge length, at about 2 m/s. All the runs were performed with the same person riding the bicycle. In this sense, it must be noted that in real-world crowdsensing applications, user behaviour can exhibit high variability regarding travelling speed, trajectory, and pauses. The standard geometries of micromobility vehicles ensure that such uncertainties are reduced in the average distribution of identified parameters. Qipei [58] proposed implementing an active filtering technique to automatically recognise and discard unstable or invalid data from subsequent analyses. Implementable solutions could consist of establishing thresholds for signal stability and consistency across acquisitions, such as minimum signal-to-noise ratios and maximum variations in frequency estimates, to exclude runs with unreliable data.

Simultaneously with each run, the smartphone placed directly on the bridge midspan acquired data. Moreover, some acquisitions were made (asynchronously) with smartphones placed on the bridge at the midspan and at about 1/4 of the bridge length (aligned with the fourth cable stay, counting from the western support). These measurements, acquired over a 5-minute period, were used to collect four separate AVTs for further benchmarking.

Regarding environmental conditions, during the field tests, the external air temperature ranged from 6 °C to 10 °C; there was no significant wind, and the weather was clear and sunny. The small temperature changes did not seem to affect the results significantly.

As for the operational conditions, since the footbridge connects two residential areas and spans over the A13 motorway, the vibrations generated by vehicular traffic beneath and around it were very

Table 1
Sensors' error variances (on the left) and process initial additive noise variance (on the right).

Measurement	Sensor variance	State Element	Sensor noise variance
Acceleration	0.01 m^2/s^4	Quaternion	$1{\cdot}10^{-1}$
Angular velocity	0.001 rad^2/s^2	Acceleration	$5{\cdot}10^{-3}$ m^2/s^4
Magnetic field	50 μT^2	Angular velocity	$3{\cdot}10^{-4}$ rad^2/s^2
Position	25 m^2	Magnetic field	$1{\cdot}10^{-1}$ μT^2
Velocity	0.001 m^2/s^2	Position	$3{\cdot}10^{-6}$ m^2
		Accelerometer bias	$3{\cdot}10^{-1}$ m^2/s^4
		Gyroscope bias	$3{\cdot}10^{-1}$ rad^2/s^2
		Compass bias	20 μT^2

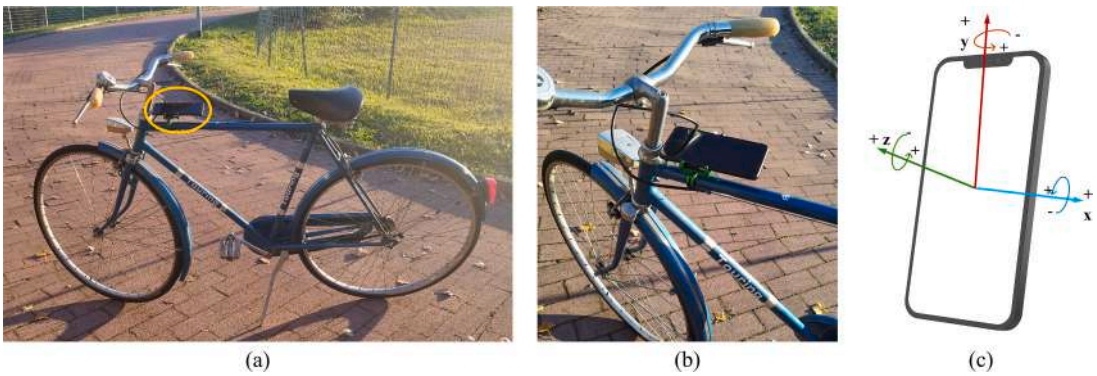

Fig. 6. Test bicycle. Side view (a), detail of the smartphone's positioning (b), and smartphone internal axes and conventions (c).

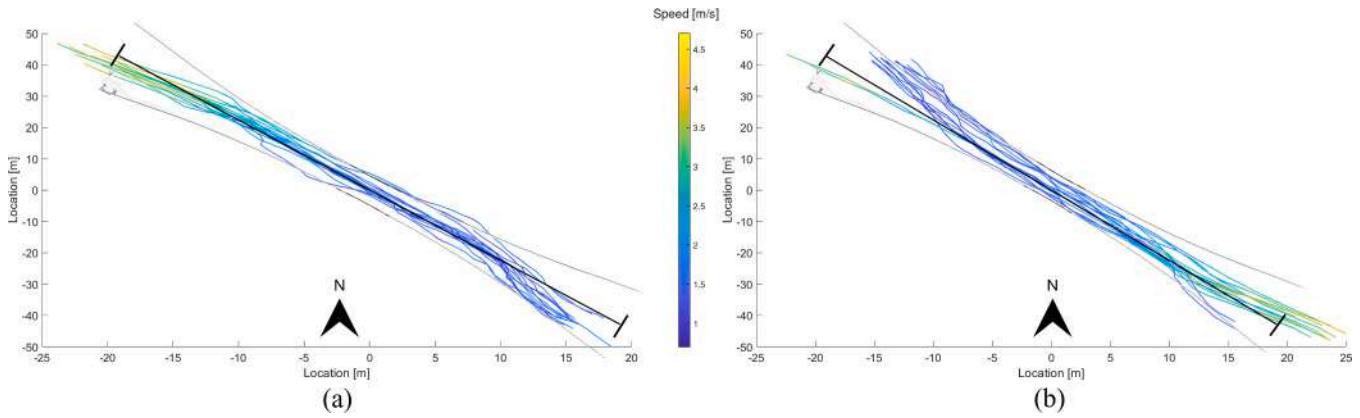

Fig. 7. Estimated travel trajectories of the bicycle in West-East (a) and East-West (b) direction with their speed (colourmap) over the footbridge plan view (in light grey) and reference bridge axis (black line). Mean velocity: 1.953 m/s; st.dev.: 0.762 m/s; range: 0.700 – 4.700 m/s.

noticeable. Additionally, the infrastructure was not closed during the tests; hence, pedestrian activity, such as walking, running, or cycling, along with the mild wind, further contributed to structural excitation during the tests.

Finally, some considerations are needed regarding vehicle-bridge and human-vehicle interactions. These were not explicitly modelled in the procedure for the following reasons. Regarding the vehicle-bridge interactions (VBI), unlike engine-propelled vehicles such as cars, motorbikes, and trucks, HPVs in general are very light and stiff, and they do not include suspensions. Hence, the bridge's vibrations are very rigidly transmitted through the bicycle's frame from the pavement to the attached sensor, as shown in [20]. Concerning the human-vehicle interactions, the presence of a cyclist influences the bicycle's dynamic behaviour. Champoux et al. [59] conducted an exhaustive dynamic analysis, revealing that the natural frequencies of the bicycle frame alone shift when a cyclist is onboard. The modal damping exhibits noticeable variations as well, across all identified modes. Without a rider, the damping ratios were found to be approximately 2 % for all identified modes, and the first bicycle natural frequency was identified at above 20 Hz with and without an onboard user. Generally, a bridge's first natural frequency is much lower than 20 Hz, especially for a relatively flexible and lightweight cycle-pedestrian bridge. Thus, according to [59], the vibration modes of the HPV, regardless of the cyclist's presence, should not influence the identification of the footbridge's modes.

4. Results

In this Section, the results obtained by applying the proposed methodology to the case study are presented and compared with those previously reported by Quqa et al. [20] on the same footbridge. Given that the two experimental campaigns were conducted nearly three years apart, this comparison also provides insights into the repeatability of the overall crowdsensing-based approach, as the infrastructure's structural conditions are known not to have changed in the meantime. Before proceeding further, it is important to note that almost all current iBSHM studies focus primarily on the first fundamental frequency or a limited number of low-frequency modes. The extraction of higher-order modes from VBI remains in its early stages, with very few studies addressing the topic, and those that do are largely theoretical in nature [60]. Therefore, to demonstrate the potential of SSI, which is the main intention of this article, modes up to 5 Hz will be presented in the following stabilisation diagrams. However, for consistency with the existing body of knowledge and, especially, due to the lack of iBSHM benchmarks beyond the first natural frequency, only the first mode will be examined in detail, although lacking reference mode shapes for direct comparison.

4.1. Results from the data of the 2023 experimental campaign

The recordings collected during the experimental test campaign conducted in December 2023 are here analysed. Regarding the drive-by measurements, obtained from the moving sensor mounted on the bicycle's front tube, the footbridge natural frequencies and damping ratios are identified using the AOMA procedure described in Section 2.1. These are compared with the benchmark values obtained by applying the same SSI identification algorithm to readings from the reference sensors installed directly on the bridge deck. The following subsections present and discuss first these results from the conventional (direct) measurements, and then those obtained through indirect drive-by monitoring, using the proposed solution.

4.1.1. Direct monitoring: Ambient vibration tests on the unloaded bridge

As mentioned, four AVTs were initially performed, with the smartphones placed directly on the bridge deck. To perform either conventional or drive-by System Identification, the AOMA procedure needs the definition of two fundamental parameters:

- The range of model orders, here set from $n_{min} = 20$ to $n_{max} = 80$;
- The number of block rows of the Hankel matrix, here defined as $2i = f_s/2$ [41].

These parameters were kept fixed for all the acquired signals to ensure fair comparability of the results. The comparison parameters for the soft validation criteria [50] were set equal to:

- $df < 0.05$
- $0 < d\xi < 10$ %

Fig. 8 shows the PSDs of the 64 vertical acceleration time series collected across all tests. Of these 64 signals:

- 30 PSDs, depicted in blue, correspond to the iBSHM data, collected from the moving bicycle;
- 30 PSDs, in purple, correspond to the synchronous acquisitions taken from the sensor directly placed on the bridge deck at mid-length;
- PSDs, in green, correspond to the AVT measurements, performed asynchronously to the bicycle runs at half and a quarter of the bridge length.

The PSDs are computed using the Welch method [61], with 4096 discrete Fourier Transform points, a Hamming window of 2048 samples, and 50 % overlap. Data are pre-processed using a third-order Butterworth bandpass filter with cutoff frequencies at 0.01 and 24 Hz, to remove near-zero drifts and high-frequency noise while ensuring that

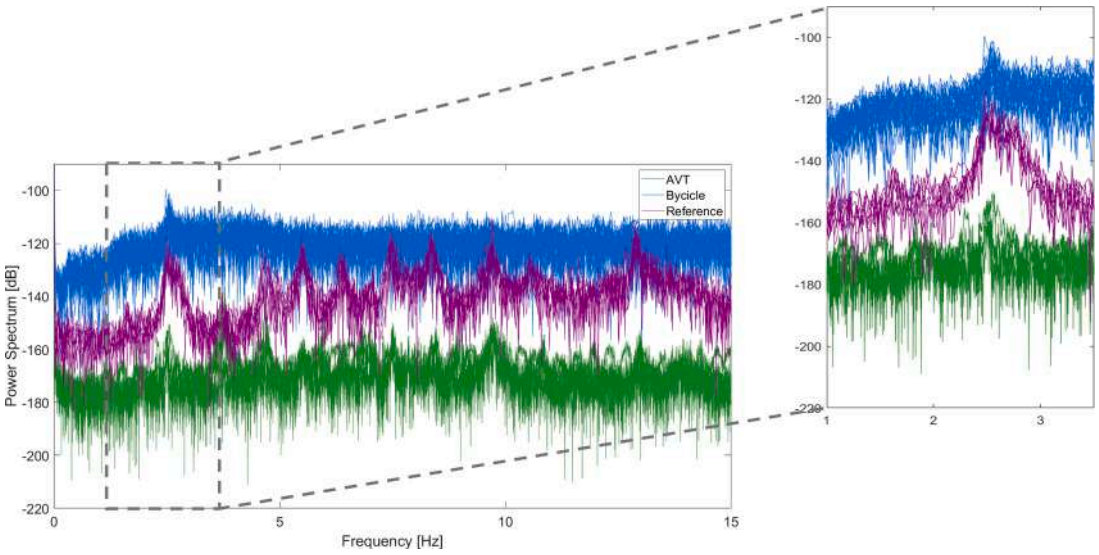

Fig. 8. PSDs related to bicycle passages (in blue), AVTs (in green), and to the reference physically-attached, stationary sensor (in purple), with a zoom view of the PSDs within the frequency range of 2–3 Hz. Power units are $(m/s^2)^2/Hz$, represented in dB, following the conversion $10\log10(P_{xx})$.

the relevant vibration modes are preserved. Observing the PSD of all signals, the first evident peak recurring in all of them is located within the range of 2 and 3 Hz. The box in the upper right corner of Fig. 8 provides a zoomed view of the frequency range of interest. The peaks visible in this zoom plot are expected, according to Quqa et al. [20], to correspond to the two modes reported in Fig. 5. It is important to notice that, due to their proximity in terms of natural frequency, the two closely spaced modes are not immediately distinguishable; consequently, the identified modal amplitudes are characterised by being a "combination of operational shapes" [20]. As it will be shown in the next Section, the two closely spaced modes appear as a single peak in the PSDs of drive-by acquisitions. In this sense, the estimated signal to sensor noise in the 2–3 Hz band is approximately 25.9 dB; however, external noises lower the signal-to-noise ratio to about −24 dB, justifying the observed merging of close peaks. Fig. 9 reports the stabilisation diagrams for the AVT performed at midspan, both in terms of natural frequencies versus model order and natural frequencies versus damping ratios. Different colours represent the clusters of stable poles.

4.1.2. *Indirect monitoring with moving sensor*

Following the same representation as in the previous Section, an example of a stabilisation diagram from iBSHM data is reported in Fig. 10. This corresponds to one signal collected by the smartphone on the bicycle during a run over the bridge. Again, the identified poles are grouped into clusters that represent the modal parameters of the structure. It was expected that, with drive-by applications, distinguishing closely spaced modes could be difficult, as confirmed in this case. Upon a first comparison with the previous stabilisation diagram from Fig. 9, the first stable mode is in good accordance with the outputs from [20], especially considering the uncertainties in the identification of the higher modes. The second cluster of poles identified (in blue) is not considered due to the negligible magnitudes of the associated singular values (see Fig. 9 (a)).

Having defined the methodology and the intermediate results for the single run, the mean frequency and damping ratio values calculated for each cluster in each acquisition (i.e., run) are then considered collectively. As expected, there is a concentration of identifications within a narrow band around 2.50 Hz, encompassing the superposition of the

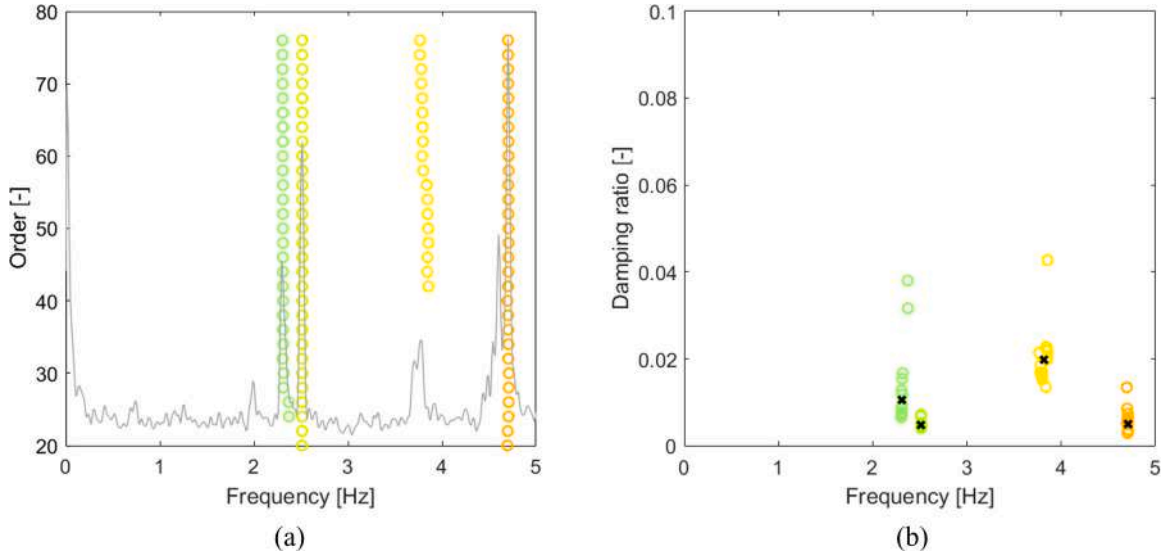

Fig. 9. Poles identified from AVT with sensor at midspan: stabilisation diagram (a) and damping vs frequency diagram (b). Each colour represents a different cluster of natural frequency-damping ratio. The black Xs represent the centroids of the respective clusters in the frequency-damping domain.

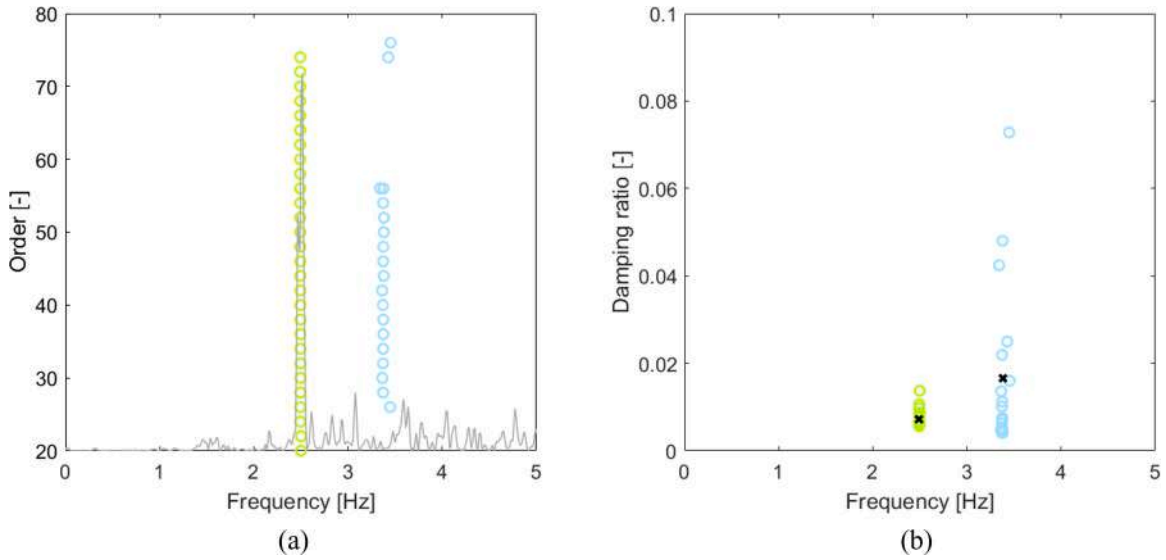

Fig. 10. Poles identified from the moving bicycle: stabilisation diagram (a) and damping vs frequency diagram (b). Each colour represents a different cluster of natural frequency-damping ratio. The black Xs represent the centroids of the respective clusters in the frequency-damping domain.

first two flexural modes. Evidently, an increase in the number of acquisitions could lead to a more robust averaging procedure, as also expected, from a crowdsensing perspective, to reduce the error in the estimated modal parameters [31]. Ideally, more acquisitions performed with the same sensor configuration would be more helpful than using multiple smartphones on the same bicycle.

4.1.3. Ablation study on AOMA parameters

To evaluate the robustness of the SSI algorithm, an ablation study was conducted on the main user-defined parameters that directly influence the reliability of its identifications. Each parameter was varied individually, while all others were kept fixed, to isolate their influence on the identifications. This process involved varying the minimum and maximum system orders, respectively as $n_{min} = 5$, 10, 20; $n_{max} = 40$, 60, 80; the number of block rows of the Hankel matrix $2i = f_s/2$, $2{\cdot}\frac{n_{max}}{n_c}$, $6{\cdot}\frac{n_{max}}{n_c}$ (n_c = number of output channels = 1 in the present case), following [41, 50]; and the stabilisation thresholds for the soft validation criterion df = 0.01, 0.05, 0.1, and dξ = 0.05, 0.1, 0.2.

For each configuration, the mean natural frequency of interest and the associated damping ratio, along with their standard deviations, and the number of identified poles N were computed over all datasets and summarised in Table 2.

As expected, the range of model orders $n = n_{max} - n_{min}$ and the number of block rows are the most influential parameters, given their role in determining the size and dimension of the system realisation [41]. Instead, the choice of dξ has little influence on the identified stable poles, while df = 0.05 is the best compromise between the number of identifications and their accuracy. The estimated average natural frequencies remain quite stable (with variation below 1.1 %); however, damping ratio estimates show larger variability, reflecting known uncertainties related to the identification of such parameter [62]. Overall, the chosen parameters ($n_{min} = 20$, $n_{max} = 80$, $2i = f_s/2$, df = 0.05, dξ = 0.1), as reported in Section 4.1.1, provided the best balance between results reliability and computational effort.

4.1.4. Operating deflection shapes and mode shapes

Here, the ODSs are extracted from the component response associated with the first flexural mode by implementing the HT as illustrated in Section 2.2. Please recall that, from an engineering perspective, these ODSs represent, by all means, an accurate approximation (up to a constant value) of the corresponding $\boldsymbol{\phi}_n$, for all the reasons already detailed in Section 2.2. To convert them from the time domain to the spatial domain, the accurate locations of the measured accelerations should be determined. Since the smartphone's sensors were triggered manually, the exact instants of entering and exiting the bridge were determined by identifying the visible amplitude peaks in the acceleration data, corresponding to the passage on the expansion joints (Fig. 11). The GPS trajectories and the bicycle trajectory estimated with the DC-EKF during an example acquisition run are reported in Fig. 12. The bridge reference line is indicated in black, with the expansion joints highlighted at both ends. The GPS measurements from the smartphone are plotted as well, in red, alongside the estimated trajectory, in blue. In addition, the hourglass shape of the footbridge deck in plan view is added (in light grey). Notably, the smartphone's GPS measurements may exhibit some

Table 2
Ablation study for the main AOMA parameters.

	$n_{min} = 5$ N = 15	$n_{min} = 10$ N = 19	$n_{min} = 20$ N = 18	$n_{max} = 40$ N = 1	$n_{max} = 60$ N = 17	$n_{max} = 80$ N = 18	i = fs/4 N = 21	$i = 2{\bullet}n_{max}/n_c$ N = 20
f_μ [Hz]	2.552	2.557	2.529	2.514	2.551	2.529	2.529	2.556
σ_f [Hz]	0.134	0.134	0.122	-	0.136	0.122	0.122	0.132
ξ_μ [%]	1.917	2.146	2.451	2.713	1.704	2.451	2.451	1.792
σ_ξ [%]	0.921	1.644	1.640	-	1.362	1.369	1.592	1.504
	$i = 6{\bullet}n_{max}/n_c$ N = 16	df < 0.01 N = 11	df < 0.05 N = 18	df < 0.1 N = 16	dξ < 5 % N = 17	dξ < 10 % N = 18	dξ < 20 % N = 17	
f_μ [Hz]	2.542	2.546	2.529	2.531	2.529	2.529	2.529	
σ_f [Hz]	0.143	0.145	0.122	0.143	0.138	0.122	0.143	
ξ_μ [%]	2.341	0.828	2.451	2.441	2.082	2.096	2.095	
σ_ξ [%]	2.624	0.417	2.525	2.624	2.371	2.369	2.369	

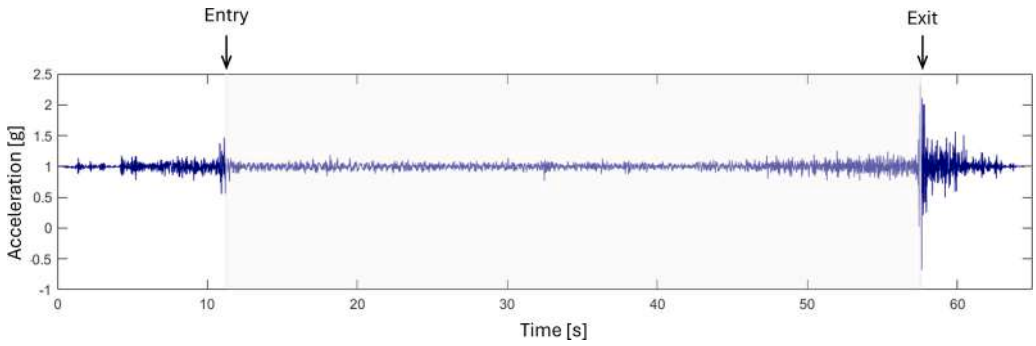

Fig. 11. Amplitude peaks identification on the vertical acceleration time history corresponding to the passage of the bicycle on the expansion joints.

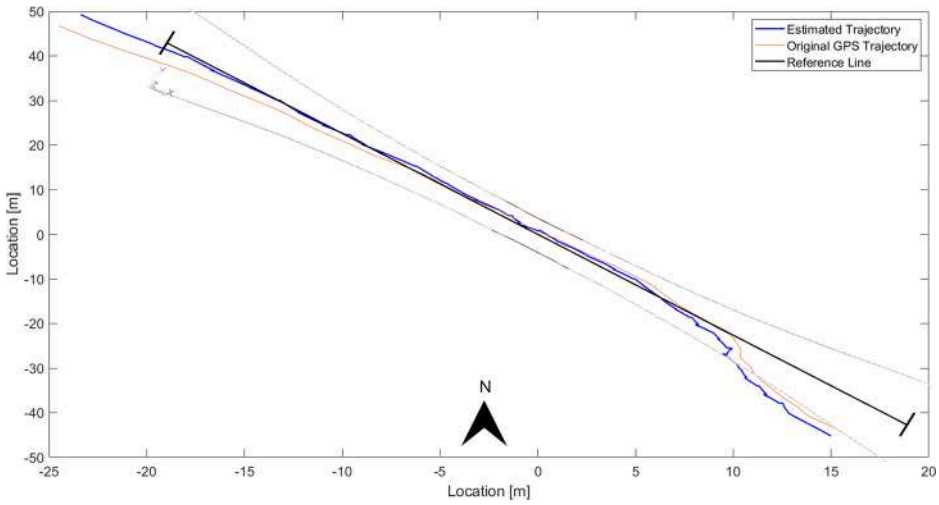

Fig. 12. GPS (in red) and estimated travel trajectory of the bicycle (in blue) over the footbridge plan view (in light grey).

inaccuracies (see Table 1), also due to the narrow width of the bridge, thus occasionally deviating from the actual path.

The results obtained for the main steps of the procedure for a single acquisition are shown in Fig. 13. After windowing the vertical acceleration history (Fig. 13 (a)), the signal corresponding to the first modal component is obtained as specified in Section 2.1 (Fig. 13 (b)). Its absolute amplitude is computed with the application of the HT, as depicted in Fig. 13 (c), which represents the signal's envelope in absolute value. Subsequently, the amplitude is interpolated with the principal components of the estimated trajectory using a spatial grid along the bridge axis (Fig. 13 (d)), consistently with the results from [20]. The initial peak visible in the estimated mode shapes is due to the effect of the passage of the bicycle on the expansion joint. This transient vibration component dissipates within 3–4 s in all the acquired time series. The procedure has been applied to all acquisitions in the dataset. From there, an average ODS value was computed to estimate the first flexural mode, as reported in Fig. 14.

4.2. Results from the data of the 2020/2021 experimental campaign

This former experimental campaign was conducted in the winter between 2020 and 2021 and used in [20], applying the procedure described there to obtain the first natural frequency and corresponding mode shape. As already mentioned throughout this paper, the main difference between Quqa et al.'s algorithm and the one proposed here lie in the methodology chosen to identify the natural frequencies, namely PP from the PSD of the vertical accelerations versus SSI, and in the use of a bandpass filter to isolate the modal components related to target frequencies (here replaced by the SVD process). From an operational point of view, the 2020/2021 experimental campaign was conducted in a very similar way to the 2023 tests. 36 runs were performed riding back and forth over the footbridge. Here, the proposed algorithm was applied to this dataset to compare results across the two campaigns and cross-validate them with Quqa et al.'s estimates.

As for Section 4.1, the occurrence of each value in terms of natural frequencies and damping ratios has been computed, and the results have been compared with those obtained from the 2023 experimental campaign. The histograms in Fig. 15 (a), Fig. 15 (b), and Fig. 15 (c) illustrate, respectively, the occurrences of the identified natural frequency for (a) the reference sensor during the 2023 campaign, (b) the moving sensor during the same, and (c) the moving sensor during the 2020/2021 tests. The computation of the mean (μ), standard deviation (σ), and standard error (SE) of the identified modal parameters across datasets provides a quantitative comparison of variability. In the subplots of Fig. 15, the vertical dotted lines represent the $\mu \pm 3\sigma$ time-invariant interval for each dataset, corresponding to a 99.7 % probability under the assumption of normally distributed properties. For the reference sensor (direct monitoring), the statistical values are respectively $f_{\mu,ref} = 2.529$ Hz, $\sigma_{f,ref} = 0.072$ Hz and $SE_{f,ref} = 0.012$ Hz computed among 37 identified values, referring to the two closely spaced modes, as stated in previous sections. Instead, for the moving sensor (2023 campaign), these are equal to $f_{\mu,2023} = 2.529$ Hz, $\sigma_{f,2023} = 0.122$ Hz and $SE_{f,2023} = 0.028$ Hz among 18 identified values. Thus, the two outcomes differ only slightly in terms of standard deviation and standard error, when viewed from a statistical crowdsensing perspective. Similarly, the results from the 2020/2021 campaign with the moving sensor show a mean frequency of $f_{\mu,2020} = 2.525$ Hz, $\sigma_{f,2020} = 0.088$ Hz and $SE_{f,2020} = 0.014$ Hz for the 40 estimates.

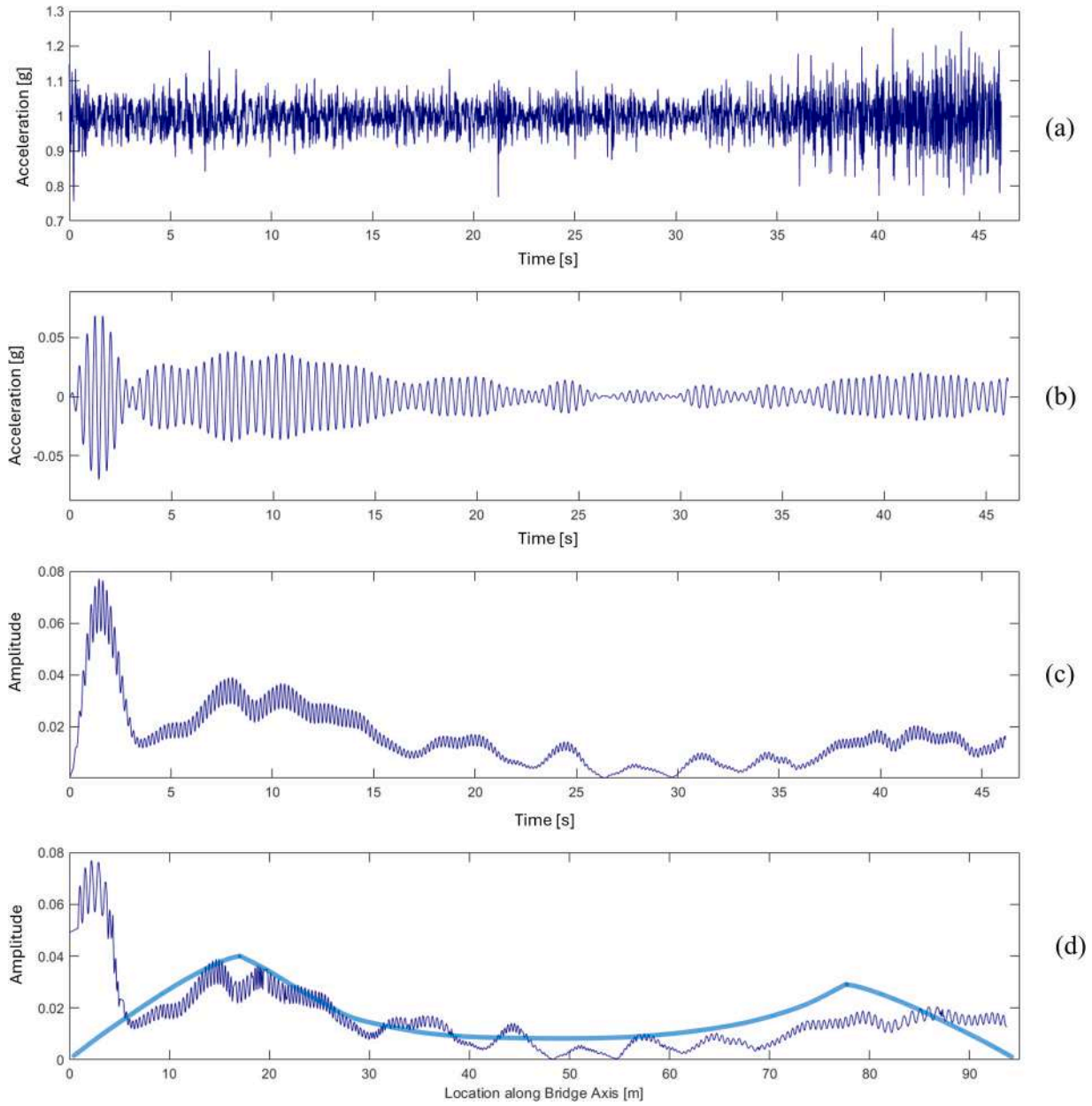

Fig. 13. Procedure workflow for mode shape estimation from a sample signal: (a) raw vertical acceleration, (b) signal related to the first modal component, (c) absolute instantaneous amplitude of the same, (d) interpolated ODS along the bridge axis superimposed to the expected mode shape, non-normalised.

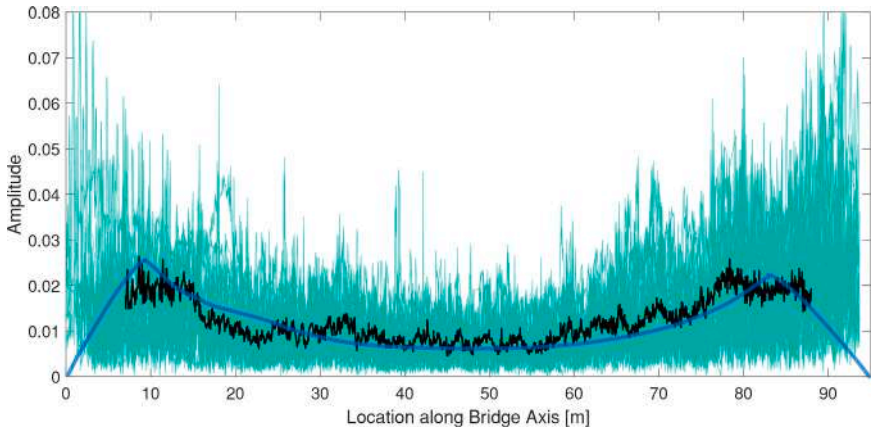

Fig. 14. Reference (blue line) and identified (black line) average non-normalised modal amplitude, superimposed on all runs (bicycle trips; in teal) for the 2023 tests.

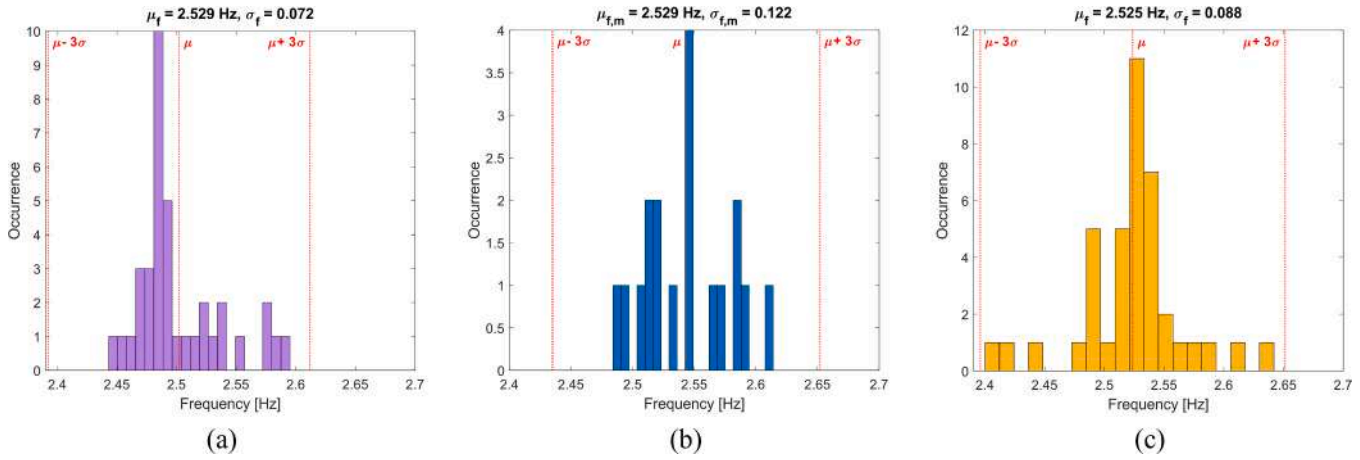

Fig. 15. Statistical distributions of the identified natural frequencies for the reference sensor (a), the 2023 experimental campaign moving sensors (b), and the 2020/21 tests moving sensors (c).

The occurrence of the identified damping ratios within the identified frequency range was similarly computed, again considering all acquisitions available for each dataset. Regarding the moving sensors, the results are respectively $\xi_{\mu,2023} = 2.451$ %, $\sigma_{\xi,2023} = 2.260$ % and $SE_{\xi,2023} = 0.371$ % for the 2023 campaign and $\xi_{\mu,2020} = 2.488$ %, $\sigma_{\xi,2020} = 2.269$ % and $SE_{\xi,2020} = 0{,}358$ % for the 2020/2021 campaign. Instead, for the reference sensor (direct monitoring, 2023), these are equal to $\xi_{\mu,ref} = 1.229$ %, $\sigma_{\xi,ref} = 0.920$ % and $SE_{\xi,ref} = 0.151$ %.

Referring to the outcomes of the original work [20], the statistical distribution of the peaks identified via PP on the PSD within the frequency range of interest was manually identified and returned a distribution characterised by a mean frequency of $f_{\mu,PP} = 2.533$ Hz, and a standard deviation $\sigma_{f,PP} = 0.035$ Hz.

4.2.1. Operating deflection shapes and mode shapes

The approximated mode shapes are retrieved employing the same methodology previously explained; hence, for conciseness, this section reports only the averaged ODS for the combination of the two closely spaced flexural modes, in absolute value, as reported in Fig. 16. The average estimated ODSs for the two experimental test campaigns have been normalised, compared, and illustrated with their respective confidence intervals, as shown in Fig. 17. These results are presented under two assumptions about the distribution of the amplitudes of the ODSs: a Normal distribution and a Rayleigh distribution [63]. Both the mean values and the corresponding intervals have been computed according to these hypotheses. In the first case, being the interval defined as $\mu \pm 3\sigma$, non-physical negative values are produced (Fig. 17 (a)), even though ODSs are positive by definition (since they come from absolute values). Under the assumption of Rayleigh-distributed values, the estimated means and the resulting confidence intervals remain positive (Fig. 17 (b)), thus ensuring a more reliable approach for reflecting the physical meaning of the modal amplitudes, even though the results, especially in terms of mean values, show a greater variability in this second case. Nevertheless, the results show robust consistency between the two experimental campaigns, confirming the robustness of the proposed identification procedure for a more comprehensive crowdsensing application that would involve different smartphones.

The good correlation between the two identified ODSs is evaluated through the Modal Assurance Criterion (MAC), which reads:

$$\mathrm{MAC}(\boldsymbol{\phi}_j, \boldsymbol{\phi}_k) = \frac{\left[\boldsymbol{\phi}_j^T \cdot \boldsymbol{\phi}_k\right]^2}{\left[\boldsymbol{\phi}_j^T \cdot \boldsymbol{\phi}_j\right]\left[\boldsymbol{\phi}_k^T \cdot \boldsymbol{\phi}_k\right]} \tag{10}$$

where $\boldsymbol{\phi}_j$ and $\boldsymbol{\phi}_k$ are the normalised mode shapes referring to the first and second experimental campaigns. In this case, the MAC obtained for the target mode (first natural frequency) is 0.941 for normally distributed values, whereas for the Rayleigh distribution it is 0.884. Evidently, the above-mentioned differences also affect this parameter. However, these values are relatively high, suggesting that the proposed methodology can be effectively used for modal identification.

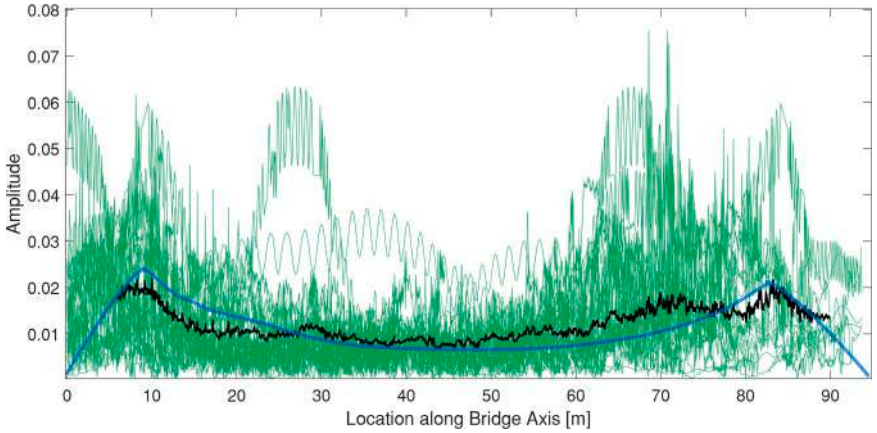

Fig. 16. Reference (blue line) and identified (black line) average non-normalised modal amplitude, superimposed on all runs (bicycle trips; in green) for the 2020/21 tests.

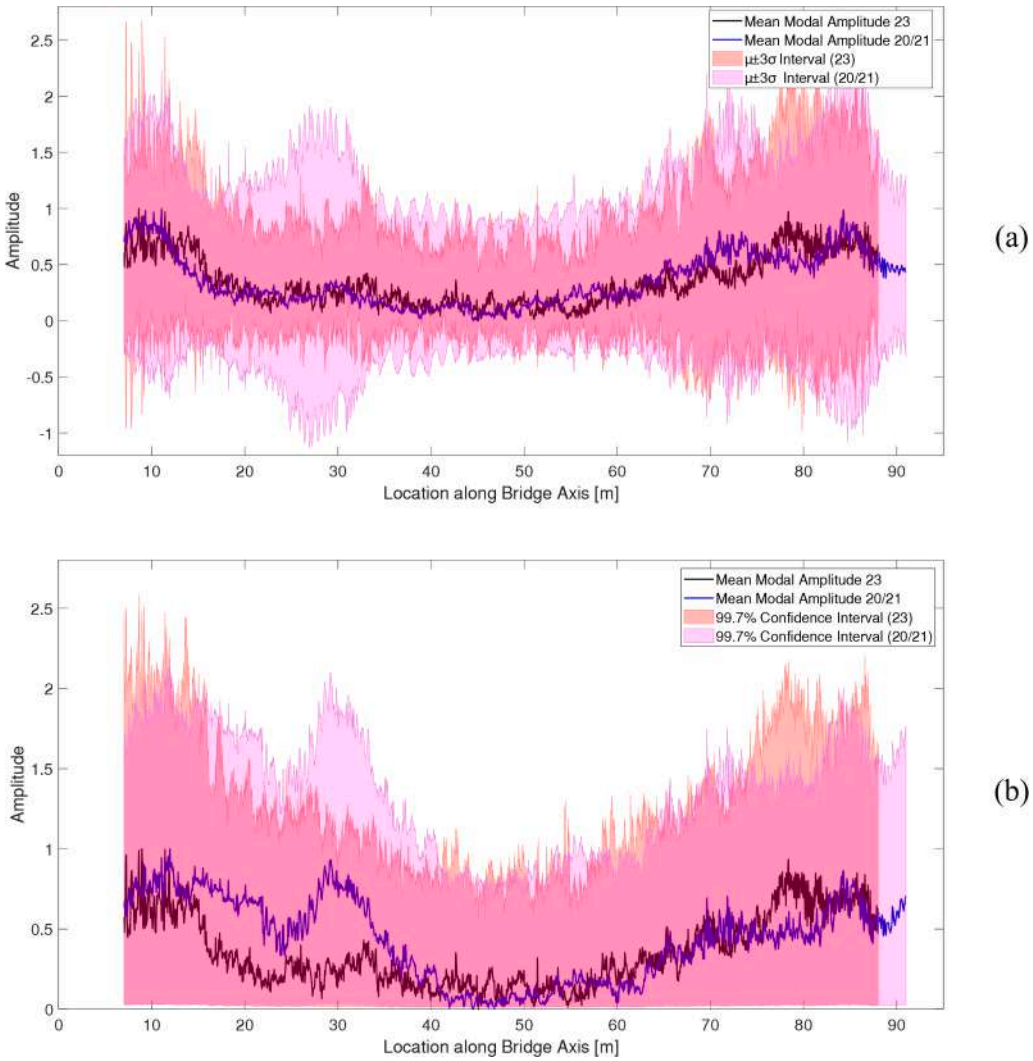

Fig. 17. Average normalised modal amplitudes (blue and black lines) superimposed to the respective confidence intervals (violet and red areas) under the assumptions of normally distributed (a) and Rayleigh distributed (b) amplitude values.

4.3. Discussion and remarks on the results

The key findings of this study are recalled here for conciseness. Regarding natural frequencies and damping ratios, all results are summarised in Table 3. These quantities reveal:

1) In terms of natural frequencies, there is a good comparability between the automated, SSI-DATA and DBSCAN-based AOMA procedure proposed here, and the Peak Picking manually performed in Quqa et al. [20], with Δf less than 0.01 Hz.
2) In terms of natural frequencies and damping ratios, there is a very good repeatability between different runs (bicycle trips) on the same

Table 3
Summary of the results.

	Quqa et al. [20] results on 2020/2021 tests	This method's results on 2020/2021 tests	This method's results on 2023 tests	Reference ground sensor, 2023 tests
OMA/AOMA algorithm	OMA: PSD - PP	AOMA: SSI-DATA + DBSCAN	AOMA: SSI-DATA + DBSCAN	AOMA: SSI-DATA + DBSCAN
f_μ	2.533 Hz	2.525 Hz	2.529 Hz	2.529 Hz
σ_f	0.035 Hz	0.088 Hz	0.122 Hz	0.072 Hz
SE_f	0.006 Hz	0.014 Hz	0.028 Hz	0.012 Hz
ξ_μ	n.a.	2.488 %	2.451 %	1.229 %
σ_ξ	n.a.	2.269 %	2.260 %	0.920 %
SE_ξ	n.a.	0.151 %	0.358 %	0.371 %
Δf	0.008 Hz		0.005 Hz	0.005 Hz
$\Delta\xi$	n.a.		0.038 %	1.222 %

experimental campaign (i.e., a relatively low variability), with $\sigma_f < 0.09$ Hz everywhere and $\sigma_\xi < 0.022$.
3) Again, in terms of natural frequencies, there is also a very good repeatability between the two experimental campaigns, performed on similar weather conditions but years apart, with Δf never larger than 0.005 Hz.
4) The natural frequency identified via drive-by (indirect) SHM is very similar to the reference sensor ($\Delta f < 10^{-4}$ Hz), while the discrepancy in terms of damping is noticeable (almost double).

All these quantitative results seem to indicate the potential feasibility of the AOMA iBSHM method for natural frequency-based damage detection, thanks to this low variability. Conversely, the variability and difference of the damping ratios hamper the viability of damping-based SHM. It can be noticed how the damping values recorded on the bicycle show greater dispersion compared to those measured directly on the bridge. Considerations about damping shall include the influence of the cyclist [64], which could introduce additional variation and cause slightly higher estimates with respect to the AVT measurements. However, ξ is generally not considered a reliable damage index in any case [50,51,62].

Finally, regarding the mode shapes, a MAC value larger than 0.94 between the two experimental campaigns is relatively good, but it would require further improvements before being reliable for mode shape-based damage detection. Nevertheless, the results of the proposed approach are well in line with current iBSHM methodologies. In this sense, to the current knowledge of the Authors, almost all full-scale tests available in the literature focus on bridge modal identification, most of which limitedly to natural frequencies extraction, rather than damage detection in general [39] and even less so for mode shape-based SHM in particular.

4.4. Limitations and future works

The proposed methodology shows promising results in identifying the set of modal parameters of the footbridge under study, leveraging crowdsourced data from smartphones mounted on HPVs. Nevertheless, some limitations need to be addressed. First of all, as already remarked, crowdsensing was simulated by performing multiple runs with the same bicycle and with a limited number of collected signals.

Although the identification steps are automated, in the present study, the data acquisition is still manually triggered, and the identification of bridge entry and exit points in each signal, corresponding to the expansion joints, was also performed manually. Future steps will include a GPS-based approach to work with bridges without expansion joints, using the vehicle's trajectory to automatically segment the signals.

The proposed approach could identify the first vibration mode (a combination of the first two closely spaced modes). Future steps will involve identifying higher-order flexural and torsional modes; however, their detection presents several challenges. Instead, the identification of lateral modes through iBSHM is still not found in the literature, principally due to uncertainties and the greater influence of lateral vehicle movements, such as steering variations, which might affect the VBI mechanics in lateral modes much more than in vertical ones.

Finally, concerning technical improvements, when dealing with larger datasets, a potential development to consider is implementing a signal filtering technique to discard unreliable or invalid data from subsequent analyses.

5. Conclusions

In this research work, an output-only, automated dynamic identification method was successfully applied to drive-by acceleration recordings. The proposed methodology combines two key components. Firstly, an Automated Operational Modal Analysis (AOMA) algorithm, based on the Data-driven Stochastic Subspace Identification Algorithm (SSI-DATA) and the Density-Based Spatial Clustering of Applications with Noise (DBSCAN), is used to estimate natural frequencies and damping ratios. In this regard, the innovation lies in the application of this AOMA procedure to the vibration time series collected by a low-cost moving sensor, a smartphone, attached to a human-propelled vehicle (HPV) – specifically, a regular bicycle. The proposed approach could identify the natural frequency (f_n) and the corresponding damping ratio (ξ_n) by taking advantage of the very fundamental passages of the SSI algorithm, replacing traditional Peak Picking on the Power Spectral Densities of vertical accelerations. Then, following a crowdsensing-based approach, data fusion between the vehicle positioning and the Hilbert Transform of the signals is used to estimate operational deflection shapes (ODSs) for each bridge crossing. These ODSs work as a good approximation of the corresponding mode shapes, completing the estimation of the full set of modal parameters. All combined, these novelties enhance automation while all returning consistent results with repeatability and accuracy across different runs, even when considering experimental campaigns performed three years apart. The comparison of the results with a previous experimental campaign showed that bridge modal parameters, particularly the first flexural mode, can be identified from the smartphone-instrumented vehicle's data in real-world operational conditions by averaging all collected datasets over a given period of time. In fact, the outcomes demonstrate consistent identification of bridge modal parameters across datasets, supporting the methodology's robustness. Considering frequencies and mode shapes as indicators of structural health, this approach potentially enables the implementation of damage detection techniques, particularly when crowdsourced data becomes available over a longer period, thanks to the widespread use of smartphones. This concept will offer less expensive solutions for urban bridge monitoring, facilitating widespread infrastructure assessment and first diagnostic scans.

Lastly, but importantly, this study focused on indirect Bridge Structural Health Monitoring with human-powered vehicles over lightweight pedestrian bridges. In this sense, the proposed method was thoroughly validated on a steel-made footbridge in Bologna, Italy. Nevertheless, the concept can be extended to engine-powered vehicles on larger road bridges; this is currently the subject of ongoing research.

CRediT authorship contribution statement

Mauro Aimar: Writing – review & editing, Validation, Formal analysis. **Maria Pina Limongelli:** Writing – review & editing, Supervision, Project administration, Funding acquisition. **Pier Francesco Giordano:** Writing – review & editing, Resources, Methodology, Data curation, Conceptualization. **Said Quqa:** Writing – review & editing, Visualization, Resources, Methodology, Data curation, Conceptualization. **Samuele Mara:** Validation, Investigation, Data curation. **Marco Raimondi:** Validation, Investigation, Data curation. **Eleonora Massarelli:** Writing – original draft, Visualization, Software, Methodology, Data curation. **Marco Civera:** Writing – original draft, Visualization, Software, Methodology, Formal analysis, Conceptualization. **Bernardino Chiaia:** Writing – review & editing, Supervision, Project administration, Funding acquisition.

Declaration of Competing Interest

The authors declare that they have no known competing financial interests or personal relationships that could have appeared to influence the work reported in this paper

Acknowledgements

M.C., M.A., and B.C. performed this work as part of the research activities within the framework of the "PNRR": SPOKE 7 "CCAM, Connected Networks and Smart Infrastructure" - WP4. This work was also part of the activities developed by M.C., S.M., M.R., P.F.G., M.A., M.P.L.,

and B.C. within the framework of the project AMBROSE (A Multisensor BRidge MOnitoring SystEm). The Italian National Centre for Sustainable Mobility (CN MOST) and Alta Scuola Politecnica are gladly acknowledged for their support.

Data Availability

Data will be made available on request.

References

[1] Farrar CR, Worden K. An introduction to structural health monitoring. Philos Trans R Soc A Math Phys Eng Sci 2007;365(1851):303–15. https://doi.org/10.1098/rsta.2006.1928.
[2] Lederman G, Chane S, Cerda F, Rizzo P, Garrett J, Noh H. Bridge Monit Technol Safe Effic Transp 2022.
[3] Yang Y-B, Lin CW, Yau JD. Extracting bridge frequencies from the dynamic response of a passing vehicle. J Sound Vib 2004;272(3–5):471–93. https://doi.org/10.1016/S0022-460X(03)00378-X.
[4] Lin CW, Yang YB. Use of a passing vehicle to scan the fundamental bridge frequencies: An experimental verification. Eng Struct 2005;27(13):1865–78. https://doi.org/10.1016/j.engstruct.2005.06.016.
[5] Sadeghi Eshkevari S, Matarazzo TJ, Pakzad SN. Bridge modal identification using acceleration measurements within moving vehicles. Mech Syst Signal Process 2020;141:106733. https://doi.org/10.1016/j.ymssp.2020.106733.
[6] Corbally R, Malekjafarian A. A data-driven approach for drive-by damage detection in bridges considering the influence of temperature change. Eng Struct 2022;253:113783. https://doi.org/10.1016/J.ENGSTRUCT.2021.113783.
[7] Yang YB, Li YC, Chang KC. Using two connected vehicles to measure the frequencies of bridges with rough surface: a theoretical study. Acta Mech 2012;223(8):1851–61. https://doi.org/10.1007/s00707-012-0671-7.
[8] Y. Fujino, K. Kitagawa, T. Furukawa, and H. Ishii, Development of vehicle intelligent monitoring system (VIMS), M. Tomizuka, Ed., 2005, p. 148. doi: 10.1117/12.601727.
[9] Benedetti L, Bernardini L, Argentino A, Cazzulani G, Somaschini C, Belloli M. Identification of bridge bending frequencies through drive-by monitoring compensating vehicle pitch detrimental effect. Struct Monit Maint 2022;9(4):305–21.
[10] Cheema P, Alamdari MM, Chang KC, Kim CW, Sugiyama M. A drive-by bridge inspection framework using non-parametric clusters over projected data manifolds. Mech Syst Signal Process 2022;180:109401. https://doi.org/10.1016/j.ymssp.2022.109401.
[11] Di Matteo A, Fiandaca D, Pirrotta A. Smartphone-based bridge monitoring through vehicle–bridge interaction: analysis and experimental assessment. J Civ Struct Health Monit 2022;12(6):1329–42. https://doi.org/10.1007/s13349-022-00593-1.
[12] Singh P, Sadhu A. A hybrid time-frequency method for robust drive-by modal identification of bridges. Eng Struct 2022;266:114624. https://doi.org/10.1016/j.engstruct.2022.114624.
[13] Gkoumas K, Gkoktsi K, Bono F, Galassi MC, Tirelli D. The way forward for indirect structural health monitoring (iSHM) using connected and automated vehicles in Europe. Infrastructures 2021;6(3):43. https://doi.org/10.3390/infrastructures6030043.
[14] Gkoktsi K, Bono F, Tirelli D. Effectiveness of drive-by monitoring in short-span bridges: a real-scale experimental evaluation. Struct Control Health Monit 2024;2024. https://doi.org/10.1155/2024/3509941.
[15] Fiandaca D, Di Matteo A, Patella B, Moukri N, Inguanta R, Llort D, et al. An Integrated approach for structural health monitoring and damage detection of bridges: an experimental assessment. Appl Sci 2022;12(24):13018. https://doi.org/10.3390/app122413018.
[16] McGetrick PJ, Hester D, Taylor SE. Implementation of a drive-by monitoring system for transport infrastructure utilising smartphone technology and GNSS. J Civ Struct Health Monit 2017;7(2):175–89. https://doi.org/10.1007/s13349-017-0218-7.
[17] Miyamoto A, Kiviluoma R, Yabe A. Frontier of continuous structural health monitoring system for short & medium span bridges and condition assessment. Front Struct Civ Eng 2019;13(3):569–604. https://doi.org/10.1007/s11709-018-0498-y.
[18] Lan Y, Li Z, Koski K, Fülöp L, Tirkkonen T, Lin W. Bridge frequency identification in city bus monitoring: a coherence-PPI algorithm. Eng Struct 2023;296:116913. https://doi.org/10.1016/j.engstruct.2023.116913.
[19] Elhattab A, Uddin N, OBrien E. Drive-by bridge frequency identification under operational roadway speeds employing frequency independent underdamped pinning stochastic resonance (FI-UPSR). Sensors 2018;18(12):4207. https://doi.org/10.3390/s18124207.
[20] Quqa S, Giordano PF, Limongelli MP. Shared micromobility-driven modal identification of urban bridges. Autom Constr 2022;134:104048. https://doi.org/10.1016/j.autcon.2021.104048.
[21] Yang YB, Xu H, Zhang B, Xiong F, Wang ZL. Measuring bridge frequencies by a test vehicle in non-moving and moving states. Eng Struct 2020;203:109859. https://doi.org/10.1016/j.engstruct.2019.109859.
[22] Yang Y, Lu H, Tan X, Chai HK, Wang R, Zhang Y. Fundamental mode shape estimation and element stiffness evaluation of girder bridges by using passing tractor-trailers. Mech Syst Signal Process 2022;169:108746. https://doi.org/10.1016/j.ymssp.2021.108746.
[23] Fitzgerald PC, Malekjafarian A, Cantero D, OBrien EJ, Prendergast LJ. Drive-by scour monitoring of railway bridges using a wavelet-based approach. Eng Struct 2019;191:1–11. https://doi.org/10.1016/J.ENGSTRUCT.2019.04.046.
[24] Urushadze S, Jong-Dar Y. Experimental investigation of a moving vehicle for identification bridge dynamic parameters. Proceedings of the 1st Latin-American Workshop on Structural Health Monitoring - LATAM SHM 2023. Dec. 2023.
[25] Yang Y-B, Chen W-F, Yu H-W, Chan CS. Experimental study of a hand-drawn cart for measuring the bridge frequencies. Eng Struct 2013;57:222–31. https://doi.org/10.1016/j.engstruct.2013.09.007.
[26] Li Z, Lan Y, Lin W. Footbridge damage detection using smartphone-recorded responses of micromobility and convolutional neural networks. Autom Constr 2024;166:105587. https://doi.org/10.1016/j.autcon.2024.105587.
[27] Massarelli E, Raimondi M, Mara S, Civera M, Aimar M, Giordano PF, et al. Output-only modal analysis and system identification for indirect bridge health monitoring: needs, requirements, and limitations 2024;515:505. https://doi.org/10.1007/978-3-031-61425-5_49.
[28] Cerda F, Garrett J, Bielak J, Rizzo P, Barrera J, Zhuang Z, et al. Indirect Struct Health Monit Bridge Scale Exp 2012. https://doi.org/10.13140/2.1.1736.0000.
[29] McGetrick PJ, Kim CW. A parametric study of a drive by bridge inspection system based on the morlet wavelet. Key Eng Mater 2013;569–570:262–9. https://doi.org/10.4028/www.scientific.net/KEM.569-570.262.
[30] Yu Y, Zhao X, Ou J. A new idea: Mobile structural health monitoring using Smart phones. 2012 Third International Conference on Intelligent Control and Information Processing. IEEE; 2012. p. 714–6. https://doi.org/10.1109/ICICIP.2012.6391524.
[31] Matarazzo TJ, Kondor D, Milardo S, Eshkevari SS, Santi P, Pakzad SN, et al. Crowdsourcing bridge dynamic monitoring with smartphone vehicle trips. Commun Eng 2022;1(1):29. https://doi.org/10.1038/s44172-022-00025-4.
[32] Cronin L, Eshkevari SS, Matarazzo TJ, Milardo S, Dabbaghchian I, Santi P, et al. Identifying damage-sensitive. Spat Vib Charact Bridges Widespread Smartphone Data 2022. https://doi.org/10.48550/arXiv.2211.01363.
[33] Feng K, Hester D, Taylor S, O'Higgins C, Ferguson A, Zhu Z, et al. Experimental modal identification of a pedestrian bridge through drive-by monitoring integrated with shared-mobility vehicles. Dev Built Environ 2024;20:100562. https://doi.org/10.1016/j.dibe.2024.100562.
[34] Abuodeh O, Redmond L. Investigation of multiple-vehicle scenarios to improve system identification for indirect health monitoring of bridge networks. Adv Bridge Eng 2025;6(1):5. https://doi.org/10.1186/s43251-024-00152-2.
[35] Cronin L, Sen D, Marasco G, Dabbaghchian I, Benedetti L, Matarazzo T, et al. A Roadmap for ubiquitous crowdsourced mobile sensing-based bridge modal identification. Sensors 2025;25(8):2528. https://doi.org/10.3390/s25082528.
[36] Peng Z, Li J, Hao H, Yang N. Mobile crowdsensing framework for drive-by-based dense spatial-resolution bridge mode shape identification. Eng Struct 2023;292:116515. https://doi.org/10.1016/j.engstruct.2023.116515.
[37] Shokravi H, Vafaei M, Samali B, Bakhary N. In-fleet structural health monitoring of roadway bridges using connected and autonomous vehicles' data. ComputAided Civ Infrastruct Eng 2024;39(14):2122–39. https://doi.org/10.1111/mice.13180.
[38] OBrien EJ, McCrum DP, Wang S. Monitoring bearing damage in bridges using accelerations from a fleet of vehicles, without prior bridge or vehicle information. Eng Struct 2024;302:117414. https://doi.org/10.1016/j.engstruct.2023.117414.
[39] Singh P, Mittal S, Sadhu A. Recent advancements and future trends in indirect bridge health monitoring. Pract Period Struct Des Constr 2023;28(1). https://doi.org/10.1061/PPSCFX.SCENG-1259.
[40] Yang YB, Lin CW. Vehicle–bridge interaction dynamics and potential applications. J Sound Vib 2005;284(1–2):205–26. https://doi.org/10.1016/j.jsv.2004.06.032.
[41] Van Overschee P, De Moor B. Subspace Identification for Linear Systems. Boston, MA: Springer US; 1996. https://doi.org/10.1007/978-1-4613-0465-4.
[42] M. Majowiecki, Un ponte ciclopedonale sulla autostrada A-13. A cycle and pedestrian bridge over the A13 motorway, 2008.
[43] Yang YB, Chen W-F. Extraction of bridge frequencies from a moving test vehicle by stochastic subspace identification. J Bridge Eng 2016;21(3). https://doi.org/10.1061/(ASCE)BE.1943-5592.0000792.
[44] Li J, Zhu X, Law S, Samali B. Indirect bridge modal parameters identification with one stationary and one moving sensors and stochastic subspace identification. J Sound Vib 2019;446:1–21. https://doi.org/10.1016/j.jsv.2019.01.024.
[45] Jin N, Dertimanis VK, Chatzi EN, Dimitrakopoulos EG, Katafygiotis LS. Subspace identification of bridge dynamics via traversing vehicle measurements. J Sound Vib 2022;523:116690. https://doi.org/10.1016/j.jsv.2021.116690.
[46] Nie Z, Xie Y, Li J, Hao H, Ma H. Damage detection in bridges under moving loads based on subspace projection residuals. Adv Struct Eng 2022;25(5):979–1001. https://doi.org/10.1177/13694332211056107.
[47] Brincker R, Andersen P. Underst Stoch Subspace Identif 2006.
[48] Reynders E, Houbrechts J, De Roeck G. Fully automated (operational) modal analysis. Mech Syst Signal Process 2012;29:228–50. https://doi.org/10.1016/j.ymssp.2012.01.007.
[49] Civera M, Sibille L, Zanotti Fragonara L, Ceravolo R. A DBSCAN-based automated operational modal analysis algorithm for bridge monitoring. Measurement 2023;208:112451. https://doi.org/10.1016/j.measurement.2023.112451.
[50] Mugnaini V, Zanotti Fragonara L, Civera M. A machine learning approach for automatic operational modal analysis. Mech Syst Signal Process 2022;170:108813. https://doi.org/10.1016/j.ymssp.2022.108813.
[51] Civera M, Mugnaini V, Zanotti Fragonara L. Machine learning-based automatic operational modal analysis: a structural health monitoring application to masonry

arch bridges. Struct Control Health Monit 2022;29(10). https://doi.org/10.1002/stc.3028.
[52] Ester M, Kriegel H-P, Sander J, Xu X. A density-based algorithm for discovering clusters in large spatial databases with noise. Proceedings of the Second International Conference on Knowledge Discovery and Data Mining. 1996. p. 226–31.
[53] Kalman RE. A new approach to linear filtering and prediction problems. J Basic Eng 1960;82(1):35–45. https://doi.org/10.1115/1.3662552.
[54] J.S. Bendat and A.G. Piersol, Random Data - Analysis and Measurement Procedures - Second Edition, url={⟨https://api.semanticscholar.org/CorpusID:172271767⟩}, 1986.
[55] Malekjafarian A, McGetrick PJ, OBrien EJ. A review of indirect bridge monitoring using passing vehicles. Shock Vib 2015;2015:1–16. https://doi.org/10.1155/2015/286139.
[56] Tan C, Uddin N, OBrien EJ, McGetrick PJ, Kim C-W. Extraction of bridge modal parameters using passing vehicle response. J Bridge Eng 2019;24(9). https://doi.org/10.1061/(ASCE)BE.1943-5592.0001477.
[57] Majowiecki M. Three footbridges. 2nd International Conference Footbridge. Venice,Italy; Dec. 2005.
[58] M. Quipei, Crowdsensing-based Monitoring of Transportation Infrastructure using Moving Vehicles, PhD Thesis, University of Alberta, 2020.
[59] Champoux Y, Richard S, Drouet J-M. Bicycle Structural Dynamics. Sound Vib 2007;41:16–24.
[60] Wang J, Chen Y, Huang Z, Tan X. High order modal extraction for bridges based on vehicle frequency changes of vehicle-bridge interaction. Comput Concr 2025;35(2):193–202.
[61] Welch P. The use of fast Fourier transform for the estimation of power spectra: a method based on time averaging over short, modified periodograms. IEEE Trans Audio Electro 1967;15(2):70–3. https://doi.org/10.1109/TAU.1967.1161901.
[62] Reynders E, Pintelon R, De Roeck G. Uncertainty bounds on modal parameters obtained from stochastic subspace identification. Mech Syst Signal Process 2008;22(4):948–69. https://doi.org/10.1016/j.ymssp.2007.10.009.
[63] M.M. Siddiqui, Statistical Inference for Rayleigh Distributions, 1964.
[64] Colmenares D, Costa G, Civera M, Surace C, Karoumi R. Quantification of the human–structure interaction effect through full-scale dynamic testing: The Folke Bernadotte Bridge. Structures 2023;55:2249–65. https://doi.org/10.1016/j.istruc.2023.06.133.